DEVELOPMENT AND MOLECULAR ANALYSIS OF CMT4B1 DROSOPHILA MODEL

by

Merve Kılınç

B.S., Molecular Biology and Genetics, Boğaziçi University, 2011

Submitted to the Institute for Graduate Studies in
Science and Engineering in partial fulfillment of
the requirements for the degree of
Master of Science

Graduate Program in Molecular Biology and Genetics
Boğaziçi University

2013

To my family…

ACKNOWLEDGEMENTS

I would like to express my sincere thanks to my thesis supervisor Prof. Esra Battaloğlu for her great supervision, guidance and encouragement during this study. I am really grateful to her for her support and trust in me. It has been a real pleasure for me to work in her lab; I have learnt a lot from her.

I would like to thank my co-advisor Assoc. Prof. Arzu Çelik for her guidance, valuable critics and endless support whenever I needed. I am very grateful to her for investing so much time and effort into this project.

I owe my special thanks to Prof. Albena Jordanova for devoting her valuable time to evaluate my thesis.

I would also like to thank Prof. Patrick Verstreken for hosting me in his laboratory to learn the techniques used in this study and conduct some of the experiments. I thank Prof. Amy Kiger for providing the fly stocks.

I would also like to express my special thanks to my lab members and friends Kerem, Kaya, Alperen, Burçak, Merve, Duygu D., Begüm, Cansu, Yıldız, Selen, Duygu K., Gamze and Özden. They've been more than a friend to me. I feel very lucky to have known them. I wish thank the members of Lab 204; Aslı, Neslihan, Mahmut Can, Balkan, Burcu, Emirhan and Harun; and also the Fly lab members; Ece, Bahar, Stefan and Güner.

I would also like to thank Jarek Kasprovicz for his help to teach me the techniques, and Sven Vilain for his help in IMAGO experiments.

Last but not least, I would like to thank my family for their unconditional love and support throughout my life. They've been always there for me.

Finally, I am grateful to TUBITAK-BIDEB 2210 for awarding and supporting me during my master.

ABSTRACT

DEVELOPMENT AND MOLECULAR ANALYSIS OF CMT4B1 DROSOPHILA MODEL

Charcot-Marie-Tooth (CMT) disease is the most common inherited disorder of the peripheral nervous system. Among about 40 genes associated with the disease, MTMR2 loss-of-function mutations are classified as CMT4B1 subtype. Its protein product belongs to the myotubularins, which are phosphatases in phosphatidyl inositol metabolism. The aim of this study was to generate a *Drosophila* model for CMT4B1 to understand the pathogenesis of this subtype by investigating how mutant MTMR2 contributes to the disease as well as furthering the current knowledge on myotubularin proteins. Firstly, already available mutant flies with partial deletion alleles of *mtm*, the fly homolog for *MTMR2*, were analyzed in terms of neuromuscular junction (NMJ) morphology and function using immunohistochemistry and FM1-43 dye uptake assays, respectively. The boutons in the NMJs, which are the connections of motor neuron terminals to muscle cells, were studied and in the NMJs of the third instar mutant larvae, excess number of satellite boutons and subboutonic structures were observed. The immunohistochemical findings with the ubiquitous and neuronal down-regulation of *mtm* showed also satellite boutons. Secondly, to generate precise deletion of *mtm* in flies, integrase-mediated approach for gene knock-out (IMAGO) was used because the targeting vector carries attachment sites, which enable the replacement of *mtm* with any gene. In this study, the *mtm*-targeting vector was prepared by cloning the homology up- and downstream sequences of *mtm* into pP{white-STAR} vector. It was randomly integrated into the X chromosome even though third chromosome was targeted. The targeting construct was tried to be mobilized; however, no recombinant flies were obtained after screening the progeny and more flies should be screened to obtain *mtm* deficient lines. Once these flies are generated, it will be possible to knock in wild type *MTMR2* and CMT-causing mutant *MTMR2* in place of *mtm* to shed light on the molecular mechanisms leading to *MTMR2*-associated neurodegeneration in CMT4B1.

ÖZET

CMT4B1 DROSOPHILA MODELİNİN GELİŞTİRİLMESİ VE MOLEKÜLER ANALİZLERİ

Charcot-Marie-Tooth (CMT) hastalığı çevresel sinir sisteminin en sık görülen hastalığıdır. Bu hastalıkla ilişkilendirilen yaklaşık 40 gen arasında, *MTMR2* mutasyonları CMT4B1 alt tipi olarak sınıflandırılmıştır. Bu genin protein ürünü, fosfatidil inositol (PI) metabolizmasında yer alan fozfatazlar olan myotubularinlere aittir. Bu çalışmanın amacı mutant *MTMR2*'nin hastalık mekanizmasındaki etkisini araştırmak amacıyla CMT4B1 için *Drosophila* modeli geliştirmektir. Öncelikle, *MTMR2*'nin sinek homoloğu olan *mtm*'in mevcut olan kısmi delesyonlu mutant sinekleri, nöromusküler morfoloji ve fonksiyon bağlamında, sırasıyla immünohistokimya ve FM 1-43 boya alımı testleriyle analiz edilmiştir. Nöromusküler bağlantılar ve nöronların uçlarının kaslarla yaptığı yuvarlak bağlantılar olan butonlar incelenmiştir. Üçüncü evredeki mutant larvaların normalde görülmeyen fazla sayıda uydu butonlara ve buton altı yapılara sahip olduğu gözlemlenmiştir. Aynı zamanda, immunohistokimya analizlerinde *mtm* anlatımının bütün organizmada ya da sinirlerde RNAi yöntemi ile seçici azaltılması sonucu da uydu butonları göstermiştir. İkinci olarak, *mtm*'in sineklerde kesin delesyonunu yaratmak ve daha sonra *mtm*'in herhangi bir genle değişimini sağlayabilmek için hedefleme vektörü ve integraz aracılığıyla gen silinmesi yöntemi (IAGSY) kullanılmıştır. Bu çalışmada, *mtm*-hedefleme vektörü, *mtm*'in alt ve üst bölgelerinin pP{White-STAR} vektörüne klonlarak hazırlanmıştır. Üçüncü kromozom hedef olarak seçilmesine rağmen, vektör X kromozomuna rastlantısal olarak entegre olmuştur. Hedefleme vektörü bu sineklerde mobilize edilmeye çalışılmış, ancak rekombinant sinek gözlenmemiştir. *mtm*-eksik sinekler elde etmek için daha fazla sinek taranmalıdır. Bu sinekler elde edildiğinde yabanıl tip *MTMR2* ve CMT'ye sebep olan mutant *MTMR2*, *mtm*'in konumuna yerleştirilerek CMT hastalığına ve MTMR2'ye bağlı nörodejenerasyona sebep olan moleküler mekanizmalara ışık tutulabilecektir.

TABLE OF CONTENTS

LIST OF FIGURES

LIST OF TABLES

LIST OF SYMBOLS

E	Glutamate
F	Phenylalenine
G	Guanine
I	Isoleucine
m	Meter
mg	Milligram
ml	Milliliter
mM	Millimolar
ng	Nanogram
Q	Glutamine
pmol	Picomole
R	Arginine
s	Second
T	Thymine
v	Volume
W	Tryptophan
w	Weight
X	Stop codon
Y	Tyrosine
Δ	Deletion
µg	Microgram

LIST OF ACRONYMS / ABBREVIATIONS

BAC	Bacterial artificial chromosome
BLAST	Basic Local Alignment Search Tool
bp	Basepair
Ca	Calcium
$CaCl_2$	Calcium chloride
Chr	Chromosome
CMT	Charcot-Marie-Tooth
DCSP	*Drosophila* cysteine–string protein
DLG	*Drosophila* discs large tumor suppressor
DNA	Deoxyribonucleic acid
EDTA	Ethylenediamine tetraacetate
EGFR	Epidermal growth factor receptor
EGR	Early growth response protein 2
ESE	Exonic splicing enhancer
FGD4	FYVE, RhoGEF and PH domain containing 4
Flp	Flippase
FM 1-43	N-(3-Triethylammoniumpropyl)-4-(4-(Dibutylamino) Styryl) Pyridinium Dibromide
FRT	Flippase recognition target
GDAP1	Ganglioside-induced differentiation-associated-protein 1
GFP	Green fluorescent protein
GRAM	Glucosyltransferase, Rab-like GTPase activators and myotubularins
GTP	Guanosine triphosphate
H_2O	Water
HA	Homology arm
HCl	Hydrochloric acid
HEPES	Hydroxyethyl piperazineethanesulfonic acid
HK1	Hexokinase 1
HL-3	Hemolymph like solution 3

HMSN	Hereditary motor and sensory neuropathy
HNPP	Hereditary Neuropathy with Liability to Pressure Palsy
HRP	Horse raddish peroxidase
IMAGO	Integrase-mediated approach for gene knock-out
IP_3	Inositol trisphosphate
kb	Kilobase
KCl	Potassium chloride
kDa	Kilodalton
LB	Luriana Bertani
Mb	Megabase
$MgCl_2$	Magnesium chloride
min	Minute
mNCV	Motor nerve conduction velocity
MTM	Myotubularin
MTMR2	Myorubularin-related protein 2
MTMR5	Myorubularin-related protein 5
MTMR13	Myorubularin-related protein 13
NaCl	Sodium chloride
$NaHCO_3$	Sodium bicarbonate
NaOH	Sodium hydroxide
NDRG1	N-myc downstram regulated 1
NEFL	Neurofilament light polypeptide
NMJ	Neuromuscular junction
PBS	Phosphate buffered saline
PCR	Polymerase chain reaction
PDZ	Post synaptic density *Drosophila* discs large and zonula occludens-1
PH	Pleckstrin homology
PI	Phosphatidyl inositol
PMP-22	Peripheral myelin protein 22
PNS	Peripheral nervous system
PRX	Periaxin
PSD-95	Post-synaptic density protein 95
PTP	Protein tyrosine phosphatase

RMCE	Recombinase-mediated cassette exchange
RNA	Ribonucleic acid
RNAi	Ribonucleic acid interference
SBF1	SET binding factor 1
SH3TC2	SH3 domain and tetratricopeptide repeats 2
shRNA	Short hair-pin ribonucleic acid
UAS	Upstream Activating Sequence
UV	Ultraviolet
Zo-1	Zonula occludens-1

1. INTRODUCTION

Charcot-Marie-Tooth (CMT) disease, also known as Hereditary Motor and Sensory Neuropathy (HMSN) is the most common inherited disorder of the peripheral nervous system (PNS) with a prevalence of 1 in 2500 (Skre *et al*., 1974). The typical clinical characteristics of CMT are progressive distal motor weakness, sensory loss, foot deformities and atrophy (Figure 1.1) (Harding and Thomas, 1980).

CMT is classified into two major subtypes according to nerve biopsy and electrophysiological findings; the demyelinating type (CMT1) that shows defects in formation and maintenance of the myelin sheath and the axonal type (CMT2), which is characterized by axonal loss. In CMT1, the median motor nerve conduction velocity (mNCV) is reduced (mNCV<38 m/s) due to impairments in the myelin sheath, and in CMT2, mNCV is normal or slightly reduced (mNCV>38 m/s) with decreased compound muscle action potential amplitudes (Dyck *et al*., 1993). An intermediate form of CMT is also identified with a mNCV between 25 and 45 m/s (Jordanova *et al*., 2006).

Figure 1.1. Clinical signs of CMT. (A-B) Loss of muscle tissue in lower extremities. (C) Typical foot deformity with a high arch (pes cavus). (D) Atrophy in hand muscles (claw hands) (taken from Pareyson and Marchesi, 2009).

Although CMT is classically categorized according to electrophysiology and nerve biopsy, since 1991 molecular genetics has been the gold standard for diagnosis and classification of CMT. The 1.4 Mb duplication in chromosome 17, that contains the gene

for *Peripheral Myelin Protein 22 (PMP22)*, was the first identified cause of CMT1A (Lupski *et al*., 1991). The duplication of *PMP22* is responsible for almost 75% of CMT1 cases. The deletion of the 1.4 Mb fragment containing the gene *PMP22* causes Hereditary Neuropathy with Liability to Pressure Palsies (HNPP) (Chance *et al*., 1993).

According to current clinical and molecular genetic data, CMT is a heterogeneous disorder; mutations identified in more than 40 genes and loci are known to be associated with CMT. It exhibits all forms of Mendelian inheritance patterns; it is inherited autosomal dominantly, autosomal recessively and X-linked dominant and recessively (Murphy *et al*., 2012). It has become clear that CMT is a very complex disease by means of different proteins involved in diverse pathways leading to disease pathogenicity. The proteins encoded by the causative genes have diverse cellular localizations and functions (Figure 1.2) (Suter and Scherer, 2003; Niemann *et al*., 2006).

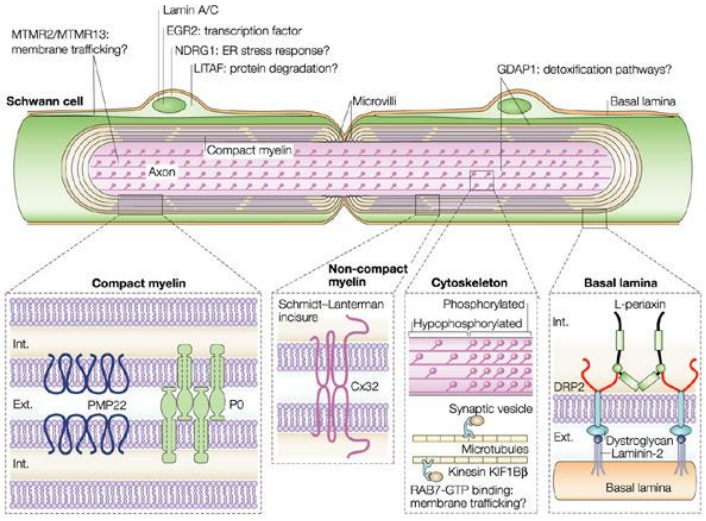

Figure 1.2. Cellular localization and function of CMT-associated proteins in PNS (from Suter and Scherer, 2003).

1.1. CMT4 Subtype: Autosomal Recessive Demyelinating CMT

CMT4 is a demyelinating subtype with autosomal recessive inheritance. Although the autosomal recessive subtypes are not common in Western Europe, the USA and Japan, they are more frequent in Mediterranean countries due to a high rate of consanguineous marriages (Dubourg *et al*., 2006).

CMT4 patients exhibit more severe clinical symptoms compared to autosomal dominant CMT cases. The disease has a very early onset, which manifests mostly before the age of 2 or 3 and has a rapid progression. CMT4 represents a broad clinical spectrum; however, the major features of CMT4 are severe disability and motor retardation, marked limb deformities such as claw-like hands in addition to pes cavus, scoliosis, hypotonia, and in some cases respiratory insufficiency, deafness and mental retardation (Barisic *et al*., 2008; Tazir *et al*., 2013). Up to now, 10 subtypes of CMT4 have been identified (CMT4A to CMT4J) and mutations in each causative gene have their own characteristic symptoms (Table 1.1).

Table 1.1. Autosomal recessive demyelinating subtypes of CMT and causative genes with their cellular functions and characteristic clinical phenotypes.

Subtype	**Gene**	**Cellular function of gene product**	**Main clinical phenotypes**
CMT4A	*GDAP1*	Mitochondrial dynamics	Hypotonia, vocal cord and diaphragm paralysis, distal muscle weakness, claw hands
CMT4B1	*MTMR2*	Membrane trafficking	Proximal lower-limb weakness, deafness, claw hands, muscle involvement, scoliosis
CMT4B2	*MTMR13*	Membrane trafficking	Glaucoma, visual impairments
CMT4C	*SH3TC2*	Endosomal recycling	Scoliosis, deafness, facial paresis, respiratory insufficiency
CMT4D	*NDRG1*	Growth arrest and cell differentiation	Deafness, tongue atrophy
CMT4E	*EGR2*	Gene regulation	Hypotonia, respiratory involvement
CMT4F	*PRX*	Myelin assembly	Sensory involvement, sensory ataxia
CMT4G	*HK1*	Glucose metabolism	Scoliosis, sensory involvement, delay in motor development
CMT4H	*FGD4*	Cytoskeletal remodeling	Scoliosis, foot deformities
CMT4J	*FIG4*	Membrane trafficking	Cranial nerve involvement

The cellular functions of proteins associated with CMT4 are diverse (Table 1.1); they are involved in mitochondrial dynamics (GDAP1), phosphatidylinositol pathway and membrane trafficking (MTMR2, MTMR13 and FIG4), endocytosis and vesicular transport (SH3TC2, NDRG1, FRABIN/FGD4), myelin structure (PRX and EGR2) and cell cycle and differentiation (NDRG1). As the proteins encoded by the CMT4 genes have diverse cellular functions, the pathomechanisms of the mutant proteins are thought to be extensive. Nevertheless, all mutations in these genes ultimately lead to a similar severe early-onset CMT phenotype.

1.2. Myotubularin Related Protein 2 (MTMR2)

Myotubularin Related Protein 2 (*MTMR2*) gene is located on chromosome 11q22 in the human genome and mutations found in *MTMR2* cause CMT subtype 4B1 (Bolino *et al*., 2000; Houlden *et al*., 2001; Nelis *et al*.; 2002, Parman *et al*., 2004; Verny *et al*., 2004). CMT4B1 is inherited autosomal recessively and has an onset in infancy. It has distinct clinical characteristics: severe disability due to distal motor and sensory neuropathy, proximal muscle weakness in lower limbs and cranial nerve affection. In some cases, patients have chest deformities, blindness and glaucoma (Tazir *et al*., 2013). mNCV in CMT4B1 has been determined to be below 20 m/s indicating that it is a demyelinating neuropathy (Quattrone *et al*., 1996). Nerve biopsy studies reveal loss of myelin sheath and areas of focally folded myelin formation in affected patients.

1.2.1. MTMR2 Belongs to the Myotubularin Protein Family

The gene product of *MTMR2* is a 643 amino acid long protein, called MTMR2. MTMR2 in humans is a member of the myotubularin (MTM) family of dual-specificity protein tyrosine phosphatases (PTPs) (Wishart and Dixon, 2002). There have been 15 identified members of human MTM phosphatases (MTM1 and MTMR1-14). Each myotubularin protein is estimated to have a particular function within the cell. Like *MTMR2*, mutations in other *MTM* genes may cause diseases; *MTM1* is associated with X-linked Centronuclear myopathy (Laporte *et al*., 1996), *MTMR13* with CMT4B2 (Azzedine *et al*., 2003), MTMR14 is a modifier for autosomal centronuclear myopathy (Tosch *et al*.,

2006). CMT 4B3 with focally folded myelin was recently associated with mutations in SET binding factor 1 (SBF1) (MTMR5) in a Korean family (Nakhro *et al.*, 2013)

The main characteristic of PTPs is the presence of a consensus catalytic HCX(5)R motif (Denu and Dixon, 1998). The cysteine (C) is the catalytically active residue; hence the MTM proteins lacking the conserved cysteine are catalytically inactive (Guan and Dixon, 1991). Nine members of MTMs (MTM1, MTMR1-4, MTMR6-7 and MTMR14) are catalytically active and the others are inactive, thus inactive MTMs cannot dephosphorylate their substrates. Nevertheless, MTM phosphatases form homo- and heterodimers, and inactive members of MTM phosphatases have a role in determining the subcellular localization of active members through their modulatory domains. For instance, MTMR2 associates with MTMR13 in human embryonic kidney 293 cells (Robinson and Dixon, 2005). MTMR13 is an inactive PTP and has been shown to be predominantly membrane-associated through its inactive phosphatase domain. It is thought to regulate the localization of MTMR2. This indicates that mutations in inactive MTMR13 might cause the CMT phenotype with focally folded myelin sheaths caused by dysregulated MTMR2 activity. The dimerization process can be exclusive among MTM-members; MTMR5 associates with MTMR2 through the coiled-coil domains, whereas it does not dimerize with MTM1, which is another active PTP (Kim *et al.*, 2003).

1.2.2. Protein Domains of MTMR2

MTMR2 has three main domains, which are also conserved in most of the MTM proteins; a pleckstrin homology - glucosyltransferase, rab-like GTPase activator and myotubularin (PH-GRAM) domain, a phosphatase domain and a coiled-coil domain (Figure 1.3 and 1.4). PH-GRAM domains bind to phosphatidyl inositol (PI) lipids, and they have a role in targeting proteins to specific cell membranes and facilitate protein-lipid and protein-protein interactions (Doerks *et al.*, 2000). The phosphatase domain dephosphorylates PIs, and the coiled-coil domain has a role in homo- and heterodimerization and membrane association (Berger *et al.*, 2003).

A conserved 80-90 amino acid sequence, a common structure in post synaptic density protein (PSD95), *Drosophila* disc large tumor suppressor (Dlg1), and zonula

occludens-1 protein (zo-1) is called PDZ-binding domain. A PDZ-binding domain is also found in many proteins and has a role in protein-protein interactions. Proteins interact with transmembrane proteins through their PDZ-binding domain at their carboxy-termini (Bilder, 2001). MTMR2 also possesses a PDZ-binding domain at the carboxy-terminal (Figure 1.4). Thus, MTMR2 might be speculated to have a role in membrane metabolism.

Loss-of-function mutations in *MTMR2* gene cause CMT4B1 phenotype with myelin outfoldings. Mutations have been found in almost all of the domains, and they result in a non-functional gene product leading to disease pathogenesis (Figure 1.4).

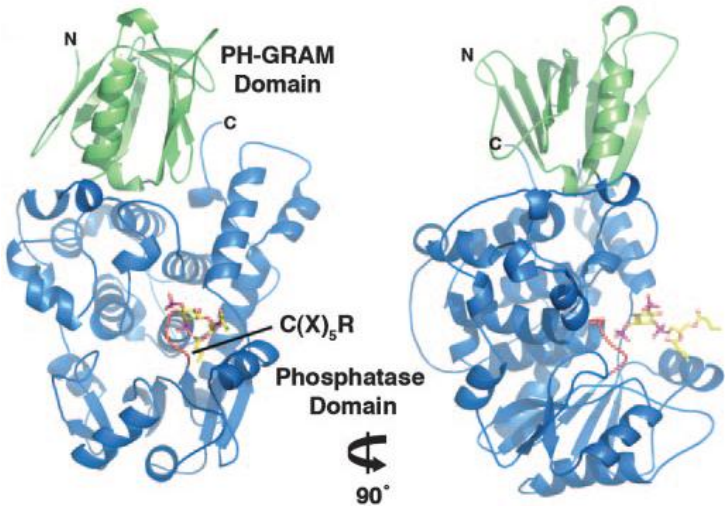

Figure 1.3. Structural organization of MTMR2 bound to its substrate PI(3,5)P_2 (from Begley *et al*., 2006).

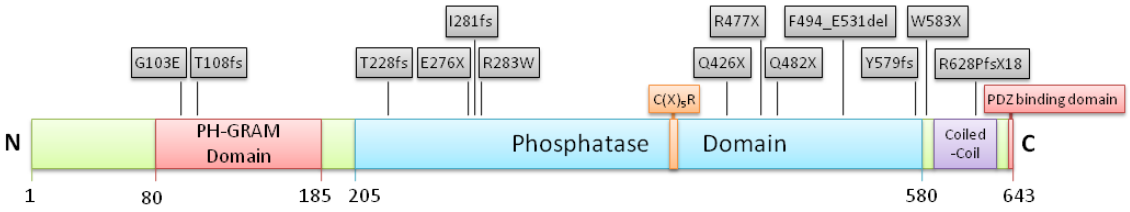

Figure 1.4. Domain organization of MTMR2 and mutations identified to cause CMT4B1 phenotype.

1.2.3. MTMR2 Has a Role in Phosphatidyl Inositol (PI) Mechanism

MTMR2 regulates PI metabolism and PIs are implicated in diverse cellular processes, such as cell signaling and membrane dynamics, cytoskeletal rearrangements, cell proliferation, differentiation, survival, autophagy and cytokinesis (Di Paolo and De Camilli, 2006; Kraus and Haucke, 2007). PI lipids are derived from phosphatidylinositol (PI) via phosphorylation of the inositol ring on different positions, and named after the position of the phosphate group (Di Paolo and De Camilli, 2006). Each PI molecule has unique subcellular localization in cellular membranes; PI3P is localized to early and late endosomes, phosphatidylinositol 4,5-bisphosphate [PI(4,5)P2] and phosphatidylinositol 3,4,5-trisphosphate [PI(3,4,5)P3] are mainly localized to the cytosolic side of the plasma membrane, and phosphatidylinositol 4-phosphate (PI4P) is predominantly found on Golgi membranes (Figure 1.5) (Di Paolo and De Camilli, 2006). PI lipids exert their function through interacting with both cellular membrane proteins and also cytosolic proteins, which have PI-recognition modules, such as PH-domains found in MTMR2.

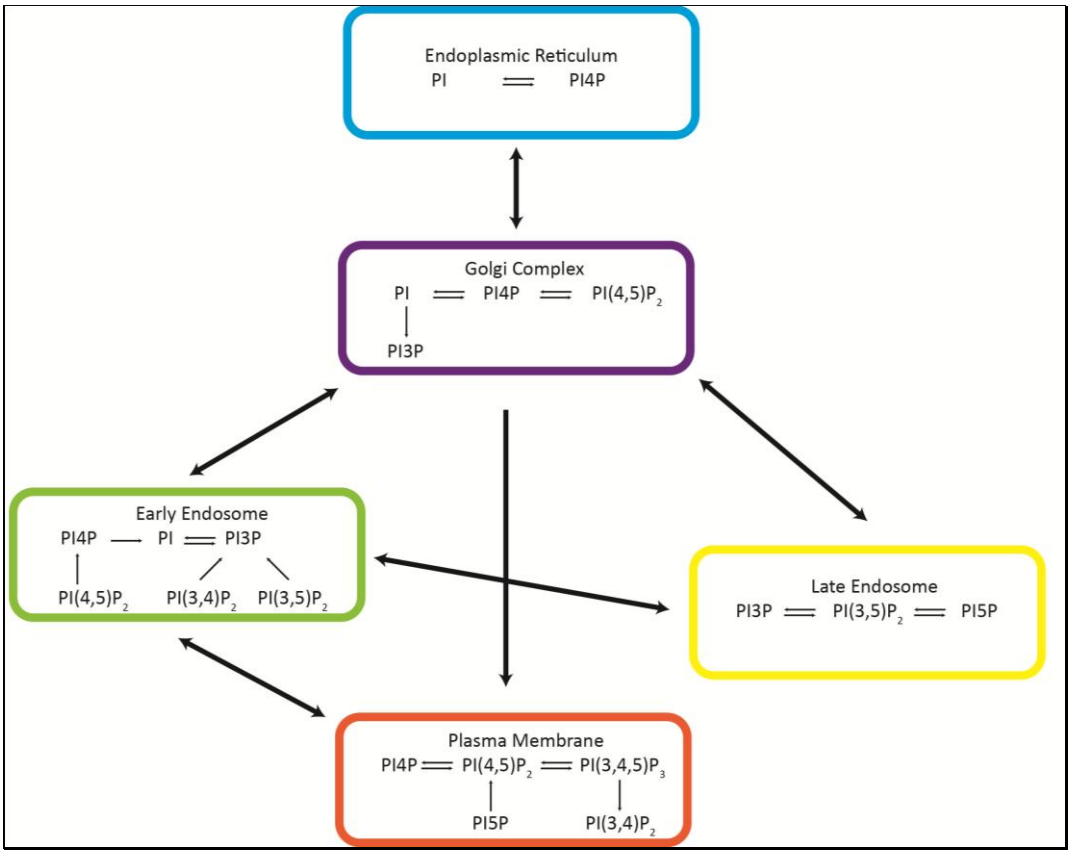

Figure 1.5. Predominant subcellular localizations of PI lipids.

It has been shown that MTMR2 possesses a phosphatase activity targeting the phosphate group on the D-3 position of the inositol ring of the phosphoinositols. MTMR2 dephosphorylates phosphatidylinositol 3,5-bisphosphate [PI(3,5)P2] and phosphatidylinositol 3-phosphate (PI3P) into phosphatidylinositol-5-phosphate (PI5P) and phosphoinositide (PI) respectively (Berger *et al*., 2002). The knock-down of MTMR2 via RNAi results in elevated levels of PI3P and accumulation of epidermal growth factor receptor (EGFR) in late endosomes. MTMR2 also co-localizes with Rab7 which is a GTPase, regulating the late-endosomal and membrane trafficking (Cao *et al*., 2008). This shows that MTMR2 might function in late endocytosis. Experimental findings suggest that MTMR2 is a negative regulator of membrane production in the case of CMT4B1; myelin outfoldings arise as a consequence of the loss of negative control on the membrane production in Schwann cells (Bolis *et al*., 2009).

1.2.4. MTMR2 Interacts with Other Proteins

The loss-of-function mutations in *MTMR2* cause myelin outfoldings in patients in the case of CMT4B1. To understand the MTMR2 mechanisms *in vivo*, a mouse model has been generated by Bolino and her co-workers (Bolino *et al*., 2004). The *Mtmr2*-null mice resembled the CMT4B1 phenotype as myelin outfoldings were observed. It was also shown that Mtmr2 interacts with Dlg1, which is expressed in Schwann cells, not in axons. The conditional down-regulation of Mtmr2 in Schwann cells results in phenotypes similar to those in Mtmr2-null mice. This shows that the Mtmr2-Dlg1 interaction might be crucial for membrane homeostasis in Schwann cells. Further evidence showed recently that Mtmr2 has a role in neurons, and Fig4 and Mtmr2 interact functionally not only in Schwann cells, but also in neurons (Vaccari *et al*., 2011). Mutations in Fig4 cause CMT4J phenotype, suggesting that Mtmr2 and Fig4 are involved in a common cellular pathway, possibly functioning antagonistically to regulate membrane formation.

It was also shown that MTMR2 that is ubiquitously expressed, interacts with neurofilament light chain (NF-L) expressed exclusively in neurons. Mutations in NF-L disrupting this interaction are responsible for axonal degeneration followed by demyelination (Previtali *et al*., 2003). It was also observed that MTMR2 directly interacts with a post-synaptic scaffolding protein, PSD-95, which is mainly localized in excitatory

synapsis in neurons (Lee *et al.*, 2010). Since mutations in MTMR2 are associated mainly with demyelinating CMT, it was thought that this pathogenic mechanism takes place mainly in Schwann cells. However, taking Vaccari and her co-workers' study into account and the interaction between NF-L, PSD-95 and MTMR2, it can be speculated that MTMR2 might have a pathogenic role not only in Schwann cells, but also in neurons.

1.2.5. Mtm Phosphatases are Conserved in Eukaryotes

MTMR2 belongs to the Myotubularin (Mtm) family of proteins, which is a large family of PTPs. Mtm phosphatases are shown to be conserved in 30 different eukaryotic species including plants, and most of the organisms are shown to possess more than one Mtm phosphatase (Figure 1.6) (Kerk and Moorhead, 2010). As mentioned earlier, humans have 15 different MTM proteins.

Considering the domain organization of Mtms, nearly all Mtms have conserved PH-GRAM and phosphatase domains in a broad range of organisms. The catalytic motif is also conserved among active Mtms. This shows that the domain organization and the catalytic consensus motif were established and conserved early in eukaryotic evolution (Kerk and Moorhead, 2010).

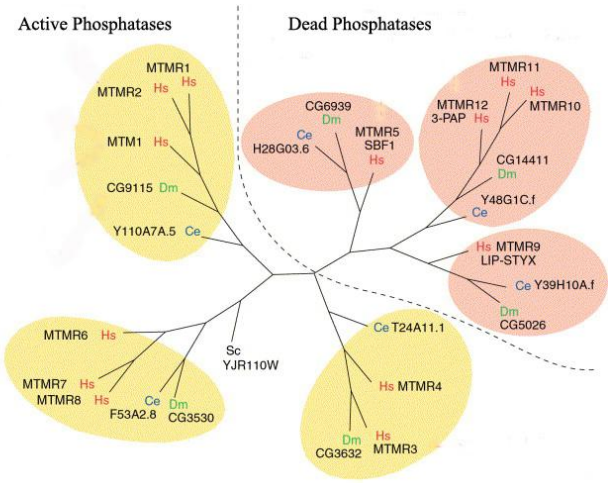

Figure 1.6. Phylogenic tree of active and inactive Mtm phosphatases from different species including human (*Homo sapiens, Hs*), fruit fly (*Drosophila melanogaster*, *Dm*) and nematode (*Caenorhabditis elegans, Ce*) (adapted from Wishart and Dixon, 2006).

1.3. *Drosophila melanogaster* as a Model Organism

The fruit fly, *Drosophila melanogaster*, has been used as an experimental model organism to study various biological processes regarding development, genetics and cell biology of eukaryotic organisms. Fundamental biological processes are conserved between human and *Drosophila*. It is also an experimentally useful model as it has a very rapid generation cycle and it can be handled easily in the laboratory.

Being million times smaller than the human brain, the fly brain has a high level of complexity of neuronal architecture (Meinertzhagen, 2010; Bullock, 1978). *Drosophila* has been widely used to study various aspects of the nervous system like neural development, neural cell biology, circuitry, behavior, learning and memory, and also the neurodegenerative disease mechanisms (Venken *et al*., 2011).

Drosophila is used as a model organism for various neurodegenerative diseases and it helps to gain insights into how genes and mutations contribute to disease mechanisms. *Drosophila* models for Amyotrophic Lateral Sclerosis, Alzheimer's, Parkinsons, Huntington's and many other diseases have been generated and the unrevealed conserved pathogenic mechanisms facilitates development of new therapies for patients (Bonini and Gitler, 2011; Moloney *et al*., 2010; Whitworth, 2011; Zala *et al*., 2012).

The *Drosophila* larval neuromuscular junction (NMJ) is a widely used model to understand neuron-muscle interactions in flies. The motor nerve terminals innervate muscles at round synaptic structures called, boutons and they permit to perform elaborate structural and functional assays to understand protein function. Using some sophisticated genetic manipulations in flies, proteins can be up- and down regulated and their effect on morphology and functioning can be analyzed. Many different types of assays can be performed using NMJ of flies. The pre- and post-synaptic localization of proteins can be analyzed by immunohistochemistry and using electron microscopy, it is possible to evaluate the number, size and the distribution of synaptic membranes (Bellen and Budnik, 2000). Electrophysiological experiments show how nerves transmit information to specific muscle groups (Imlach and McCabe, 2009). N-(3-Triethylammoniumpropyl)-4-(4-(Dibutylamino) Styryl) Pyridinium Dibromide (FM1-43) dye uptake assays reveal

information about endo- and exocytosis and vesicle trafficking taking place in the synapses (Verstreken *et al*., 2008).

The *Drosophila melonagaste*r genome was fully sequenced in 2000 and thereafter became a very useful model organism, since it provides the most elaborate genetic manipulation systems (Adams *et al*., 2000). Among many different genetic tools that have been generated to manipulate the fruit fly genome, the yeast Gal4-UAS (Upstream Activating Sequence) binary system, *P*-element-mediated transgenesis and site-specific recombination via Flp-FRT system are the most commonly used ones (Greenspan, 2004; Venken and Bellen, 2005). These techniques allow the researchers to do functional genomics and understand eukaryotic biological processes.

1.3.1. The Gal4-UAS Binary System in *Drosophila*

The Gal4-UAS system is the most commonly used method to manipulate the expression levels of genes (Duffy, 2002). Gal4 is a 881 amino acid protein, identified in *Saccharomyces cerevisiae*. Upon induction by galactose, Gal4 regulates the transcription of genes by binding to their 5'- regulatory sequences, called Upstream Activated Sequences (UAS) Element (Giniger *et al*., 1985).

Following the observation that transgenic expression of Gal4 in *Drosophila* did not have any deleterious effects, Gal4-UAS binary system was adapted for spatial and temporal expression of a target gene in *Drosophila* (Fischer *et al*., 1988, Brand and Perrimon, 1993). The gene of interest is cloned downstream of UAS-elements, and its expression is silent in the absence of Gal4. Gal4 is expressed using tissue and developmental stage-specific regulatory elements, which are together called drivers. In this system, the Gal4 driver and the UAS elements should be found in one genotype in order to interact and express the gene of interest in the desired tissue and at the time of interest (Figure 1.7).

The inhibition of gene expression through RNA interference (RNAi) can be also achieved by the Gal4-UAS binary system. A genome-wide transgenic RNAi library has been established for *Drosophila* (Dietzl, *et al.,* 2007). The RNAi transgenes, which encode

short fragments of gene sequences, are located downstream of UAS-elements. These transgenes are expressed using the Gal4-UAS binary system. The short hairpin RNA (shRNA) molecules targeting the gene of interest activate cellular mechanisms to down-regulate the target gene's expression. This system is utilized for loss of function analyses of genes in any tissue and developmental stage in *Drosophila*.

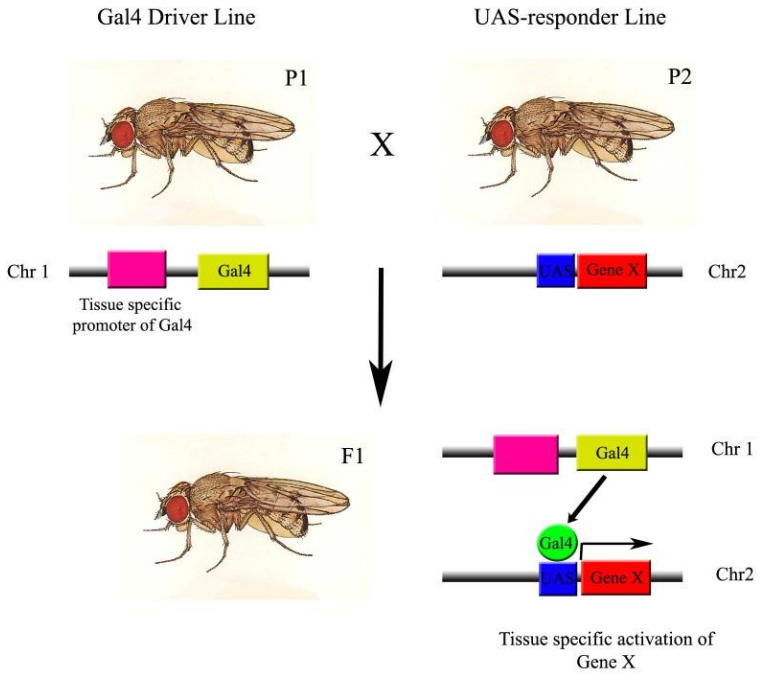

Figure 1.7. Gal4-UAS binary system. The Gal4 driver line, P1, has a *Gal4* sequence downstream of a tissue specific promoter. The UAS-responder line, P2, has Gene X downstream of an UAS-element.

1.3.2. Imprecise Excision of *P*-Elements

Transposable elements are DNA sequences, which can be mobilized in the genome and P-elements, a type of transposable elements, are widely used in *Drosophila* genetics for mutagenesis, transgenesis, deletions and gene tagging (Venken and Bellen, 2005). Since the *Drosophila* genome has been fully sequenced, it is possible to determine the *P*-element insertion sites genome-wide.

P-elements can be used to generate mutations in the insertion site. A *P*-element may be inserted into the proximity of a gene of interest, thereby generating a null allele. The *P*-transposase is activated to catalyze the excision of the *P*-element generating a double-strand break. Then the cellular repair mechanisms recover the double-strand break; consequently, some of the DNA sequences flanking the insertion site are deleted and this may lead to the generation of a stable null allele (Adams and Sekelsky, 2002).

1.3.3. Gene Targeting by Homologous Recombination

Homologous recombination is a versatile method which has been widely used in yeast and mice for targeted gene replacement. In both systems, a linear DNA fragment is inserted into cells, and the targeted gene is replaced by a substitute gene in the inserted linear DNA fragment. For a long time, the method was not usable in *Drosophila* because a germ-line stem-cell culture could not be established. Instead, circular DNA fragments can be introduced into the fly genome by microinjection into embryos (Adams and Sekelsky, 2002).

Recently, Rong and Golic have generated a method to carry out homologous recombination in *Drosophila* utilizing the fly's endogenous machinery for DNA repair and recombination (Rong and Golic, 2000). In this method, the donor construct has four main structures: a marker gene, up- and downstream homology sequences flanking the targeted gene, Flippase-Recognition-Target (FRT) sequences which help the vector to flip out from the genome upon Flippase (Flp) activity and a recognition site for *I-Sce*I restriction nuclease (Bi and Rong, 2003). The marker gene is flanked by the homology arms of the gene of interest, which are themselves flanked by FRT and *I-Sce*I sites (Figure 1.8).

The donor construct is injected into the *Drosophila* genome by P-element transformation, and it is excised out by the activity of Flp. The excised circular donor is cut by the *I-Sce*I and forms a linear DNA fragment ready for homologous recombination. The linear DNA fragment, which has homologous sequences of the flanking regions of the gene of interest, recombines with the flanking homology regions of the gene of interest. Finally, the gene of interest is replaced with the genetic marker, generating a knock-out allele for that gene (Figure 1.8).

Choi and co-workers generated a useful model to generate a conditional mutagenesis model for *Drosophila*, called integrase-mediated-approach for gene knock-out (IMAGO) (Choi *et al.*, 2009). In this system, the flippase is expressed in a certain tissue, not ubiquitously, and this permits the tissue-specific deletion of the target gene. Another important point of their study is the use of *attP* integrase sites, which flank the marker gene. This creates a ΦC31-integrase-exchangeable cassette so that the marker can be replaced by any gene flanked by *attB* integrase sites. A knock-in construct having the *attB* sites can replace the marker gene upon ΦC31 integrase activity (Figure 1.9).

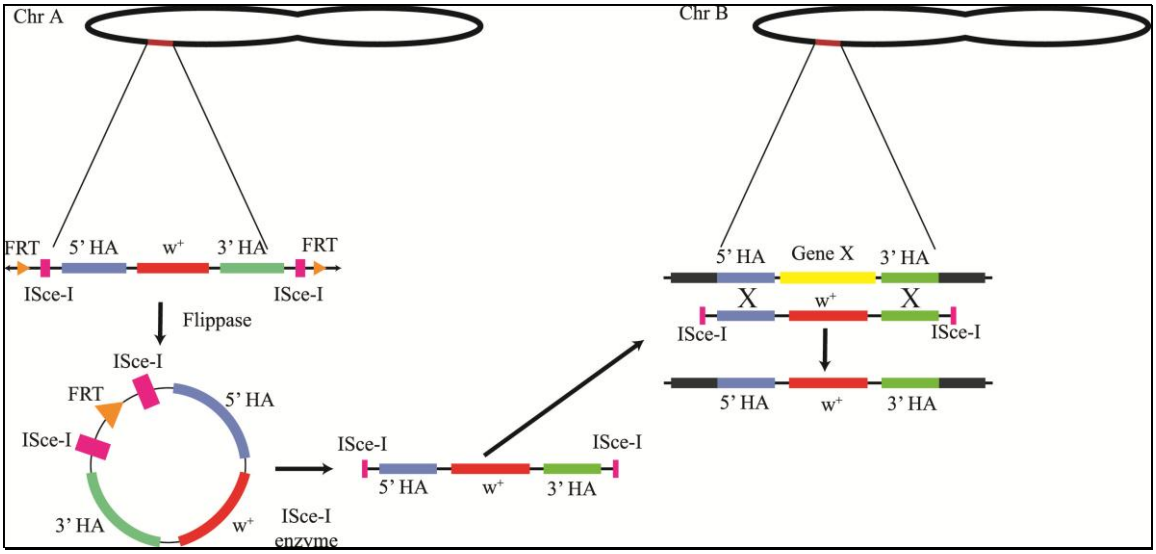

Figure 1.8. Gene targeting via homologous recombination.

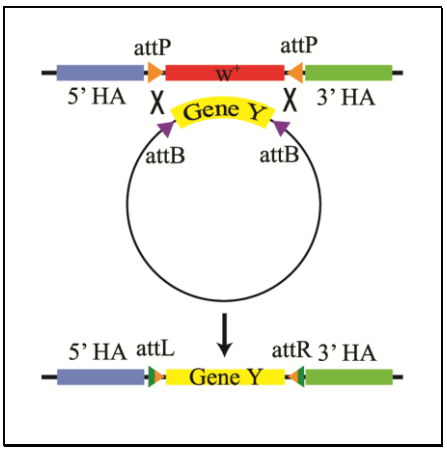

Figure 1.9. Recombinase-mediated cassette exchange (RMCE).

Gene targeting by homologous recombination is a valuable method to study disease models, since genes can be deleted or replaced without disrupting other genes. This way it is also possible to understand whether the bioinformatically found homolog is a functional homolog of the disease-causing gene. One can generate deletions and analyze its effects in flies, and rescue the phenotype by expressing the human homolog of the gene of interest. It is also possible to knock-in disease-causing mutant forms of the gene. Thereby, it can be concluded whether the generated fly model is a suitable organism to do further functional research.

2. AIM OF THE STUDY

MTMR2 is a CMT-causative gene and its gene product has been shown to have a role in PI-homeostasis and membrane trafficking. It is expressed ubiquitously; nevertheless, mutations affect specifically the peripheral nervous system, causing the CMT4B1 phenotype. The role of MTMR2 in CMT pathogenesis still remains unclear.

In this study, our aim is to understand the role of MTMR2 using *Drosophila melanogaster* as a model organism. MTMR2 is a highly conserved protein among eukarya, and *Drosophila* has a homolog, called myotubularin (mtm).

In the first part of the study, to establish the techniques and initiate use of model flies in functional analysis of CMT genes in our laboratory, we aimed to analyze the morphological differences in NMJs between wild type and *mtm*-null flies that have been previously generated by *P*-element excision. The techniques established for this purpose were immunohistochemical and FM 1-43 dye uptake assays do detect morphological and functional changes, respectively, in neuromuscular junction (NMJ) of *Drosophila*. The results are expected to be verified by down-regulation of *mtm* using *Drosophila* RNAi lines.

In the second part, we designed and performed experiments to produce a *Drosophila* model for CMT4B1 *via* deleting *mtm* by precise gene targeting using integrase-mediated approach for gene knock-out (IMAGO). These flies will further be used to knock-in wild type and mutant *MTMR2* to understand whether *mtm* recapitulates the symptoms of MTMR2.

3. MATERIALS

3.1. Biological Material

All the fly stocks were kept in incubators set to 25 °C with a 12:12 day:night cycle and 80% humidity, unless otherwise stated. Drosophila melanogaster lines used in the study and their relevant phenotypes and genotypes are listed in Table 3.1.

Table 3.1. List of *Drosophila melanogaster* lines used in the study.

Name of Line	**Chr. No**	**Description**
w^{1118}	I	White eye
yw	I	Yellow body color and white eye
yv	I	Yellow body color and vermillion eye
CyO	II	Balancer chromosome
CyO, Roi	II	Balancer chromosome with rough eye
CyOteriGFP	II	Balancer chromosome with GFP expression
TM3,hs:hid	III	Balancer chromosome, heat shock lethal
GlaBc	II	Phenotypic marker with glazed eye
$mtm^{\Delta 77}$	II	Null mutant allele of *mtm*
$mtm^{\Delta 210}$	II	Null mutant allele of *mtm*
$mtm^{z2\text{-}4747}$	II	Null mutant allele of *mtm*
hs:Flp,hs:I-SceI	III	Expresses flippase and I-SceI upon heat shock
ey-Flp	III	Expresses flippase under control of eyeless promoter
UAS-Dcr	I	Expresses Dicer-2 under UAS control
UAS-mtmTRIP	III	Expresses double stranded RNA of *mtm* under UAS control
actin5C-Gal4	II	Expresses Gal4 ubiquitously
OK6-Gal4	II	Expresses Gal4 in motor neurons
n-Syb-Gal4	III	Expresses Gal4 in synapses in the pattern of the neuronal synaptobrevin gene.

3.2. Chemicals

3.2.1. Enzymes

Phusion High-Fidelity DNA Polymerase was purchased from New England Biolabs. Bio-X-Act was purchased from Bioline. Zero Blunt TOPO PCR cloning kit was purchased from Life Technologies.

3.2.2. Chemical Supplies

The list of all chemical supplies are listed in Table 3.2.

Table 3.2. List of chemical supplies.

1 kb DNA Ladder	Thermo Scientific, USA (#SM0311)
1 kb Plus DNA Ladder	Life Technologies, USA (10787-018)
Ethidium Bromide solution	Sigma Life Sciences, USA (E1510)
Agarose	Prona Agarose, Biomax, EU (124543PR)
Tris	Sigma-Aldrich, USA, (T1503)
Sodium Acetate	Merck, Germany (1.06265)
EDTA	Sigma-Aldrich, USA (34549)
NaCl	Sigma-Aldrich, USA (S7653)
KCl	Merck, Germany (TA741635)
$NaHCO_3$	Sigma-Aldrich, USA (S7277)
HEPES	Sigma-Aldrich, USA (H4034)
Sucrose	Sigma-Aldrich, USA (S0389)
Trehalose	Sigma-Aldrich, USA (T9531)
$MgCl_26H_2O$	Carlo Erba Reagenti, (7791186)
$CaCl_2$	Sigma-Aldrich, USA (4901)
FM1-43	Life Technologies, USA (T-3163)
PBS	Life Technologies, USA (70011-044)
Triton X-100	Sigma-Aldrich, USA (T8787)
Formaldehyde	Sigma-Aldrich, USA (47608)

Table 3.2. List of chemical supplies (cont.).

Normal goat serum	Sigma-Aldrich, USA (G9023)
VectaShield mounting medium	Vector Laboratories, USA (H-1000)
Silicone Elastomere Kit	Fisher Scientific, UK (NC9644388)
LB-Broth	Difco, France, (244620)
LB-Agar	Difco, France (244520)
Ampicillin	Mustafa Nevzat, Turkey (Ampisina)
Chloramphenicol	Applichem, Germany(7495)
Kanamycin	Life Technologies, USA (11815-024)

3.2.3. Buffers and Solutions

The contents of the solutions used in this study were listed in Table 3.3 and Table 3.4.

Table 3.3. Contents of solutions that were used for NMJ assays.

Buffer/ Solution	**Content**
HL-3 Solution	110 mM NaCl 5 mM KCl 10 mM $NaHCO_3$ 5 mM HEPES 30 mM Sucrose 5 mM Trehalose 10 mM $MgCl_2$ (pH=7.2)
Fixation Solution	3.7% Formaldehyde Solution in HL3
PBX	1X PBS 0.4% Triton X-100
Blocking Solution	10% Normal Goat Serum in PBX

Table 3.3. Contents of solutions that were used for NMJ assays (cont.).

Buffer/ Solution	**Content**
Stimulation Solution	50 mM NaCl 90 mM KCl 10 mM $NaHCO_3$ 5 mM HEPES 30 mM Sucrose 5 mM Trehalose 10 mM $MgCl_2$ 2 mM $CaCl_2$ (pH=7.2)
FM1-43 Labeling Solution	4 μM FM1-43 in Stimulation Solution

Table 3.4. Contents of solutions used in molecular biology experiments.

Buffer/ Solution	**Content**
LB Broth	5 g/l NaCl 10 g/l Tryptone 5 g/l Yeast extract
LB Agar	5 g/l NaCl 10 g/l Tryptone 5 g/l Yeast extract 15 g/l Agar
P1(Resuspension Buffer)	50 mM Tris-Cl, p H 8.0 10 mM EDTA 100 μg/ml RNase A
P2 (Lysis Buffer)	200 mM NaOH 1% SDS (w/v)
P3 (Neutralization Buffer)	3.0 M Potassium Acetate, pH 5.5
Elution Buffer	10 mM Tris-Cl, pH 8.5
1X TAE Buffer	40 mM Tris-HCl 1 mM EDTA 0.1% Acetic acid
Ethidium Bromide Solution	10 mg/ml

Table 3.4. Contents of solutions used in molecular biology experiments (cont.).

Buffer/ Solution	Content
1% Agarose Gel	1X TAE Buffer 1% Agarose 0.5% Ethidium Bromide

3.2.4. Oligonucleotide Primers

Lyophilized primers were resuspended in distilled sterile water with a final concentration of 100 mM and stored at -20°C. The sequences of primers used in this study are listed in Table 3.5.

Table 3.5. Sequences of primers used in the course of this study.

Primer Name	Primer Sequence (5'→ 3')	T_m°C
CG9115_5HF	ggtaCCAGGCATACTGTGCGATTC	59.6ºC
CG9115_5HR	cctaGGTGATACCGACCCGTCC	60.7ºC
CG9115_5H_S1	CAACTTACTCTTGCGATGACTG	53.6ºC
CG9115_5H_S2	CGCTGAATAAATGTCCGCTC	54.1ºC
CG9115_5H_S3	AGTTGATGCCCACCGAGAG	57.2ºC
CG9115_5H_S4	AGCTGAAGCTGACGCACTC	57.8ºC
CG9115_5H_S5	GGCTAGAGCGTTATCGTTG	53.1ºC
CG9115_5H_T1	GCGCAGGATCAGTGTATG	56.1ºC
CG9115_5H_T2	TGCGAGTGCGTCAGCTTCA	59.5ºC
CG9115_5H_T3	TCCGCTTGTGTGTAGGAAC	57.3ºC
CG9115_5H_T4	CTGCAACACATACTGGTCA	55.2ºC
CG9115_5H_T5	TCATCGGTTGTGCGGAGA	56.1ºC
CG9115_3HF	ccgcGGCACGTTCATTGGGACAG	65.0ºC
CG9115_3HR	ccgcGGAATGCACAGAGTTGCGAC	64.7ºC
CG9115_3H_S1	CCTATATCCTGTGCCTCCTC	53.9ºC
CG9115_3H_S2	CGGAGAAATGGCTGTGTAAG	53.5ºC
CG9115_3H_S3	CGGGCAATTAAACCGAATGG	54.7ºC
CG9115_3H_S4	TACAGACCGCTGCTGATCC	56.9ºC

Table 3.5. Sequences of primers used in the course of this study (cont.).

Primer Name	**Primer Sequence (5'→ 3')**	**T_m°C**
CG9115_3H_S5	CGACGGCTTCAACTACCAC	59.5ºC
CG9115_3H_T1	GTGTGGTAGTTGAAGCCGTC	60.5ºC
CG9115_3H_T2	ATTGAGTCTCACCTCAGCA	55.2ºC
CG9115_3H_T3	GGATGATATGGTTGTGTGGA	56.4ºC
CG9115_3H_T4	CATGCAGCAGACAAGGCA	56.1ºC
CG9115_3H_T5	CTTCGCAACAGAGCACCA	55.6ºC

* lowercase letters indicate the nucleotides which do not anneal to the corresponding template; yet, the nucleotides are found in restriction endonuclease cut sites.

3.2.5. Antibodies

Antibodies used in this study are listed in Table 3.6.

Table 3.6. Primary and secondary antibodies used in the study and their properties.

Name	**Antigen**	**Host**	**Dilution**	**Company**
Primary Antibodies				
4F3 anti-DLG1	Discs large	mouse	1:50	DSHB
Anti-DCSP-2	Cysteine –string protein	Mouse	1:100	DSHB
Anti-HRP	Horse raddish peroxidase	Rabbit	1:1000	Jackson Laboratories
Anti-Synorf1	Synapsin	Mouse	1:100	DSHB
Secondary Antibodies				
Alexa 488	Rabbit	Goat	1:500	Invitrogen
Alexa 555	Mouse	Goat	1:500	Invitrogen

3.3. Disposable Labware

Disposable labware used in this study are listed in Table 3.7.

Table 3.7. Disposable labware used in the study.

Labware	**Brand**
Centrifuge tubes, 15 ml	Becton, Dickinson and Company, USA
Centrifuge tubes, 50 ml	Becton, Dickinson and Company, USA
Culture tubes, 14 ml	Greiner Bio-One, Belgium
Filter tips	Fisher Scientific, UK
Microcentrifuge tubes, 0.5 ml	Fisher Scientific, UK
Microcentrifuge tubes, 1.5 ml	Fisher Scientific, UK
Microcentrifuge tubes, 2 ml	Fisher Scientific, UK
Microscope cover glass	Isolab, Germany
Microscope slides	Isolab, Germany
Microseal PCR sealers	Bio-Rad, USA
PCR tubes (200 µl)	Fisher Scientific, UK
PCR strips (8 well)	Fisher Scientific, UK
PCR plates (96 well)	Fisher Scientific, UK
Petri dishes (60 mm)	Isolab, Germany
Petri dishes (90 mm)	Isolab, Germany
Pipette tips	Fisher Scientific, UK

3.4. Equipment

Automated DNA sequencing was conducted by Macrogen, Korea. A Nikon FN1microscope with an Intensilight (C-HGFI, Nikon) light source was used in FM 1-43 dye uptake assays performed in the imaging facilities of University of Leuven (Belgium).

The equipments used in the experiments that were performed in our department are listed in Table 3.8.

Table 3.8. Equipments used in the study.

Equipment	**Brand**
Autoclave	Astell Scientific Ltd., UK
Centrifuges	Centrifuge 5415 (Eppendorf, Germany)

Table 3.8. Equipments used in the study (cont.)

Equipment	**Brand**
Cold Room	Birikim Elektrik Soğutma, Turkey
Confocal Microscope	SP5-AOBS (LEICA, USA)
Dissection Forceps	FST, USA
Dissection Microscope	SZ61 (Olympus, Japan)
Dissection Scissors	Vannas Fine Scissors (WPI, USA)
Electrophoresis Equipment	Mini-Sub Cell (Bio-Rad, USA) PROTEAN Vertical Electrophoresis System (Bio-Rad, USA)
Fluorescence Stereomicroscope	MZ16FA (Leica Microsystems, USA)
Freezers	-20 ºC Bosch, Germany -20 ºC Arçelik, Turkey -70 ºC (Thermo Forma, USA
Gel Documentation System	Gel Doc XR (Bio-Rad Labs, USA)
Heating Block	DRI-Block DB-2A (Techne, UK)
Heating magnetic stirrer	Speed Safe (Hanna Instruments, USA) MK 418 (Nüve, Turkey)
Fly Incubators	TK 120 (Nüve, Turkey) TK 600 (Nüve, Turkey)
Laboratory Bottles	Isolab, Germany
Micropipettes	Gilson, USA
Microwave oven	Arçelik, Turkey
Refrigerators	+4º C Arçelik, Turkey
Shaker	SL 350 (Nüve, Turkey)
Stereo Microscope	Olympus, USA (SZ61)
Thermal Cycler	Bio-Rad Labs, USA (C1000 Thermal Cycler)
Vortex Mixer	Nuvemix (Nüve, Turkey)
Water Bath	BM 302 (Nüve, Yurkey)

4. METHODS

4.1. Histological Methods

4.1.1. Larval NMJ Dissection

Dissection pins were stuck on silicone plates and HL-3 solution was added onto the plate. A third instar larva was placed onto the plate containing the HL-3 solution. A dissection pin was pushed through the anterior part of the larva and another pin was pushed through the posterior part. The larva was stretched a bit longitudinally and stabilized by sticking pins into the silicone. A hole in the middle of the larva was opened by poking the dorsal cuticle with the sharp side of another pin. Starting from the hole, the larva was cut open longitudinally between the dorsal tracheas. Then, the gut and fat tissue were removed carefully. It is important not to touch the ventral muscles, brain and nerves bundles. The larva was spread open by sticking four other dissection pins in each corner. So, the ventral muscles of the third instar larva were exposed. The remaining fat tissues, trachea and gut were removed. The preparation was washed once more with fresh HL-3. The motor nerves projecting from the ventral nerve cord were cut carefully, without touching the ventral muscles.

4.1.2. Immunohistochemistry

The third instar larvae dissected as described above were fixed with 3.7% formaldehyde in HL-3 for 20 minutes. The fixation solution was discarded and the preparation was washed two times with HL-3. Starting from the posterior side, the dissection pins were removed carefully. Larvae of different genotypes are labeled by cutting the posterior end of one genotype and put together into one test tube containing 1 ml 0.4% PBX solution. The samples were washed 4 times for 15 minutes. The non-specific binding sites were blocked by incubating the larvae in blocking solution for 1 hour. The tissues were incubated with primary antibodies overnight at 4 ºC overnight. Antibody solutions were prepared by diluting antibodies in desired concentration in the blocking solution.

Next day, the antibody solution was removed and the preparations were washed with PBX five times for 10 minutes. The secondary antibody solution was prepared diluting antibodies in blocking solution, and the larvae were incubated with secondary antibodies for 2 hours at room temperature in the dark. The samples were washed in PBX for 2 hours changing solutions every 15 minutes.

Finally, the samples were prepared for microscopy. A drop of Vectashield was put on a microscope glass and larvae were put into this mounting medium. Ventral muscles and brain were located on top. A cover-glass was put gently onto the preparation and the edges were sealed with nail polish. All immunohistochemistry preparations were kept at 4 ºC.

4.1.3. FM1-43 Dye Uptake Assay

One control and one mutant third instar larva were picked and dissected in HL-3 as described. The HL-3 solution was removed and replaced by FM 1-43 labeling solution to stimulate endo- and exocytosis. The samples were incubated for five minutes on 225 rpm shaker at dark. FM 1-43 solution was removed and the samples were washed 3-4 times over 5 minutes with HL-3 to stop the stimulation and remove the not-internalized dye. The labeled boutons were imaged under a fluorescent microscope with a 40X water immersion lens.

4.1.4. Quantitative Analysis of NMJ

After immunohistochemistry, the microscopy slides were visualized in Leica Confocal microscope using LAS AF software. The images obtained were processed and analyzed using ImageJ 1.45S software. The lengths of NMJs were measured and its ratio to innervated muscle area was determined for each NMJ. The mean values of compared using two-tailed t-test .

In order to evaluate FM 1-43 dye uptake assay, the level of fluorescence intensity was calculated using Amira 2.2. software and two-tailed t-test was used for statistical analysis.

4.2. Molecular Biology Techniques

4.2.1. Isolation of BAC DNA

The genomic BAC clone, BACR10M11, including *mtm* was purchased from BACPAC CHORI. A sterile pipette tip was dipped into the stab culture, and streaked onto a chloramphenicol plate. After incubation overnight at 37 ºC, single colonies were obtained. Five single colonies were randomly selected and 50 ml LB cultures were inoculated and grown overnight.

To extract BAC DNA, the solutions of GeneJET Plasmid Miniprep Kit (Thermo Scientific) were used. The cultures in 50 ml tubes were centrifuged at 3500 rpm for 10 minutes. The supernatant was discarded and the pellet was resuspended in 750 µl of P1 solution. 750 µl of P2 solution was also added to each tube and the mixture was gently shaked. After incubation at room temperature for 5 minutes, 1050 µl of P3 solution was slowly added. The tubes were placed on ice for five minutes. Centrifugation was performed using a Beckmann JA-14 rotor with 10000 rpm at 4 ºC for 15 minutes, and the supernatants were transferred to new 15 ml centrifuge tubes and 2250 µl of ice-cold isopropanol was added. The tubes were placed on ice for 15 minutes and the BAC DNA was precipitated by centrifugation in Beckman JA-14 rotor with 10000 rpm at 4 ºC for 15 minutes. The supernatant was removed and the pellet was washed with 70% ethanol. The pellet was air-dried for 30 minutes and the DNA was resuspended in 500 µl elution buffer.

4.2.2. Isolation of Plasmids

Plasmids were isolated using GeneJET Plasmid Miniprep Kit (Thermo Scientific), according to the manufacturer's instructions. Briefly, colonies were grown on 5 ml LB cultures overnight. On the next day, the bacteria were spun down at 3500 rpm for 5 minutes in bench top Eppendorf Microcentrifuge. The pellet was resuspended in 250 µl P1 solution, and 250 µl P2 solution was added. After mixing, 350 µl P3 solution was added and gently mixed. The tubes were centrifuged at 13000 rpm for 10 minutes, and the supernatant was transferred to spin columns of the kit. The columns were centrifuged for 1 minute, and the flow-through was discarded. The column was washed twice with 500 µl

wash solution. The plasmids were eluted by adding 50 µl elution buffer and centrifugation for 2 minutes.

4.2.3. Transformation of Plasmid DNA

Chemically competent *Escherichia coli* (*E. coli*) TOP10 strain were thawed on ice, and 2 µl of a ligation product was added and mixed gently. The bacteria were incubated for 30 minutes on ice, and the cells were heat-shocked for 90 seconds at 42 ºC. The tubes were transferred to ice and 500 µl LB medium was added. The bacteria were incubated at 200 rpm at 37 ºC for one hour. About 20-100 µl of each transformation were spread on selective agar plates and incubated at 37 ºC overnight. On the next day, colonies were picked for further analysis.

4.2.4. Restriction Digestion

BAC or plasmid DNA was digested using relevant restriction endonucleases, according to the manufacturer's instructions. Generally, 2 µg DNA was digested by 10 units of enzyme for 1 hour at 37 ºC in a reaction volume of 50 µl. The reaction was stopped by heat inactivation if possible or by agarose gel electrophoresis. DNA fragments were separated on 1% agarose gel.

4.2.5. Ligation of DNA Fragments

Two vectors were used to clone DNA fragments; pCR-Blunt II TOPO to clone PCR fragments and pP{WhiteStar}, which constitutes the P-element vector backbone for our targeting vector. For pCR-Blunt II TOPO reactions, the manufacturer's instructions were applied. Briefly, 2 µl of blunt ended PCR products were incubated with 1 µl of vector and salt solution with a final volume of 6 µl at room temperature for 5 minutes and competent cells were transformed with the reaction product.

For pP{WhiteStar} ligations, the vector was cut by relevant restriction endonucleases as described above, and the DNA fragments with compatible ends were ligated using T4 DNA ligase (Roche). The molar insert:vector ratio was chosen as 3:1. One µl of vector

was used in the ligation reaction with a final volume of 10 µl and the reaction was incubated at 16ºC overnight. The competent cells were transformed as described.

4.2.6. High Fidelity PCR

High fidelity PCR was performed to amplify the upstream and downstream sequences of *mtm*. The genomic BAC clone, BACR10M11, was used as template. The primer pairs, CG9115_5HF- CG9115_5HR and CG9115_3HF- CG9115_3HR, were used to amplify ~ 3.2 kb upstream and downstream regions of *mtm*, respectively. PCR was performed in a total volume of 50 µl for each region, using the chemicals described below (Table 4.1).

The conditions of the reaction are given in Table 4.2. In the first five cycles of the reaction, the annealing temperature was set as 2 ºC lower than the melting temperature of the complementary nucleotides, as the 5' ends do not complement with the template. In the next 30 cycles, the annealing temperature was set as 2-8 ºC lower than the annealing temperature of the primers. For this reaction, Phusion High-Fidelity DNA Polymerase was used to generate homology arms of *mtm* with no mutations.

Five µl of each reaction and 1 µl of agarose loading buffer was loaded on a 1% agarose gel to analyze the size of the amplicons. The rest of the reactions were pooled in one tube and loaded into one well in order to extract the amplicon of the desired size.

Table 4.1. Contents of high fidelity PCR.

Contents	**Volume**	**Final Concentration**
Template	2.0 µl	4 µg/ml
5X Phusion Buffer	10.0 µl	1X
DMSO	1.5 µl	3%
dNTP (10 µM)	1.0 µl	0.2 µM
Forward Primer (10µM)	1.0 µl	0.2 µM
Revese Primer (10µM)	1.0 µl	0.2 µM
Sterile H_2O	to final volume 50 µl	

Table 4.2. Cycling conditions for high fidelity PCR.

(i) Initial denaturation	98 °C	1 min
(ii) Denaturation	98 °C	30 sec
(iii) Annealing	54 °C	20 sec
(iv) Extension	72 °C	80 sec
Repeat the steps (ii)-(iv) 5x		
(v) Denaturation	98 °C	30 sec
(vi) Annealing	57 °C	20 sec
(vii) Extension	72 °C	80 sec
Repeat the steps (v)-(vii) 30x		
(viii) Final extension	72 °C	10 min
(ix) Cooling	4 °C	1 h

4.2.7. Colony PCR

Colony PCR was performed in order to screen for positive transformant colonies after bacterial transformation. Colonies were picked with a sterile pipette tip and dipped into an empty sterile PCR tube. Primer pairs were chosen according to insert and vector. PCR was performed in a total volume of 20 µl, using the chemicals described below (Table 4.3). The PCR conditions were givedn in Table 4.4.

Five µl of each reaction and 1 µl of agarose loading buffer was loaded on a 1% agarose gel and analyzed under UV illumination.

Table 4.3. Contents of colony PCR.

Contents	**Volume**	**Final Concentration**
Bio-X-Act Mixture (2X)	10.0 µl	1X
Forward Primer (10µM)	0.5 µl	0.25 µM
Revese Primer (10µM)	0.5 µl	0.25 µM
Sterile H_2O	to final volume 20 µl	

Table 4.4. Cycling conditions for colony PCR.

(i) Initial denaturation	95 °C	5 min
(ii) Denaturation	95 °C	30 sec
(iii) Annealing	variable	30 sec
(iv) Extension	72 °C	20 sec/kb
Repeat the steps (ii)-(iv) 30x		
(v) Final extension	72 °C	10 min
(vi) Cooling	4 °C	1 h

4.2.8. Gel Extraction of DNA

In order to isolate DNA fragments after a PCR or restriction digestion reaction, all the reaction mixture was loaded on a 1% agarose gel. After separating DNA fragments, their sizes were compared to a DNA ladder and the correctness of the size was confirmed. The desired DNA fragment was cut from the agarose gel with a sterile razor blade under UV light. The gel containing the DNA was put into a tube, and Agarose Gel Extraction kit (Roche) was used to extract DNA according to manufacturer's instructions.

4.3. Experiments for Down-Regulation of *mtm* in *Drosophila*

4.3.1. *P*-Element Excision Mutants

In order to study the function of mtm in flies, Velichkova and co-workers generated *mtm*-deficient flies using *P*-element excision (Velichkova *et al*., 2010). They generated the null excision alleles ($mtm^{\Delta 77}$ and $mtm^{\Delta 210}$) and a point mutation in the catalytic HCX_5Rmotif ($mtm^{z2\text{-}4747}$) that were kindly donated to our laboratory. The second chromosome on which mtm is located was balanced over a GFP-tagged balancer chromosome CyO-teriGFP. The compound heterozygous larvae were selected according to the crossing scheme in Figure 4.1.

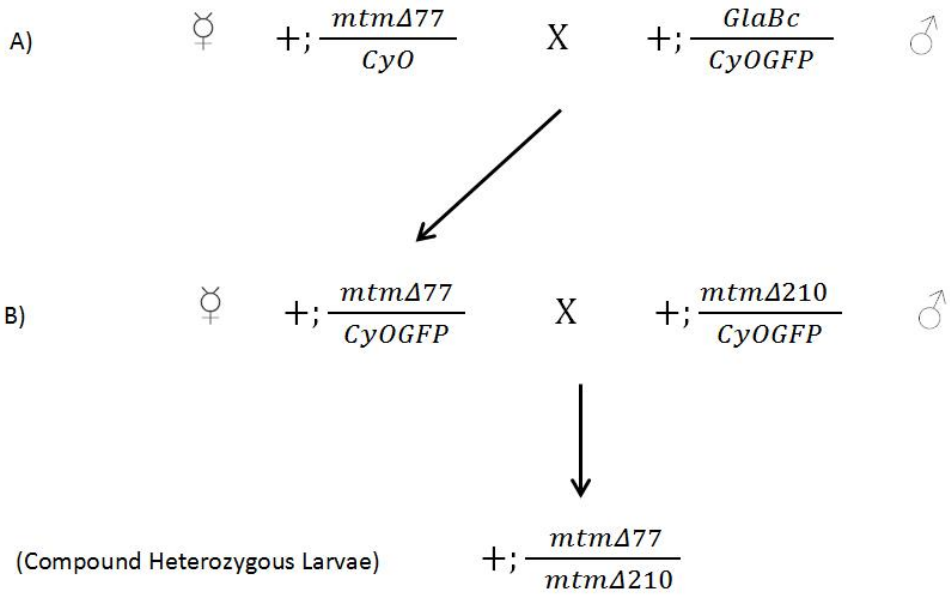

Figure 4.1. *mtm*-null alleles were rebalanced over the balancer chromosome CyO-GFP, and the non-fluorescent compound heterozygous larvae were selected against GFP background.

4.3.2. Tissue Specific Down-Regulation by RNAi

The RNAi line for *mtm*, UAS-mtmTRIP was ordered from the Bloomington Stock Center. The double-stranded RNA of *mtm* was expressed *via* ubiquitous, motor neuronal and synaptic drivers (Figure 4.2). The flies were kept at 29 ºC except UAS-Dicer;;n-Syb-Gal4 crosses. For control experiments, the control driver lines were crossed into a yv background. The flies were then analyzed by immunohistochemistry.

4.3.3. Targeting *mtm via* Homologous Recombination

In order to knock-out *mtm* from Drosophila, the targeting vector, pP{white-STAR}, was sent to Genetic Services, Inc., USA, an injection company. Flies having an attachment site, *attP2*, on their third chromosome were selected. The vector was injected into *Drosophila* embryos.The vector carried a red eye marker (w^+) was injected into flies with white eye color background, so the injection can be tracked in the progeny by checking the eye color, as red eye is dominant over white eye.

The male flies which have red eye were collected and the chromosome of the injection site was detected by crossing the flies with quadruple-balancer virgin flies.

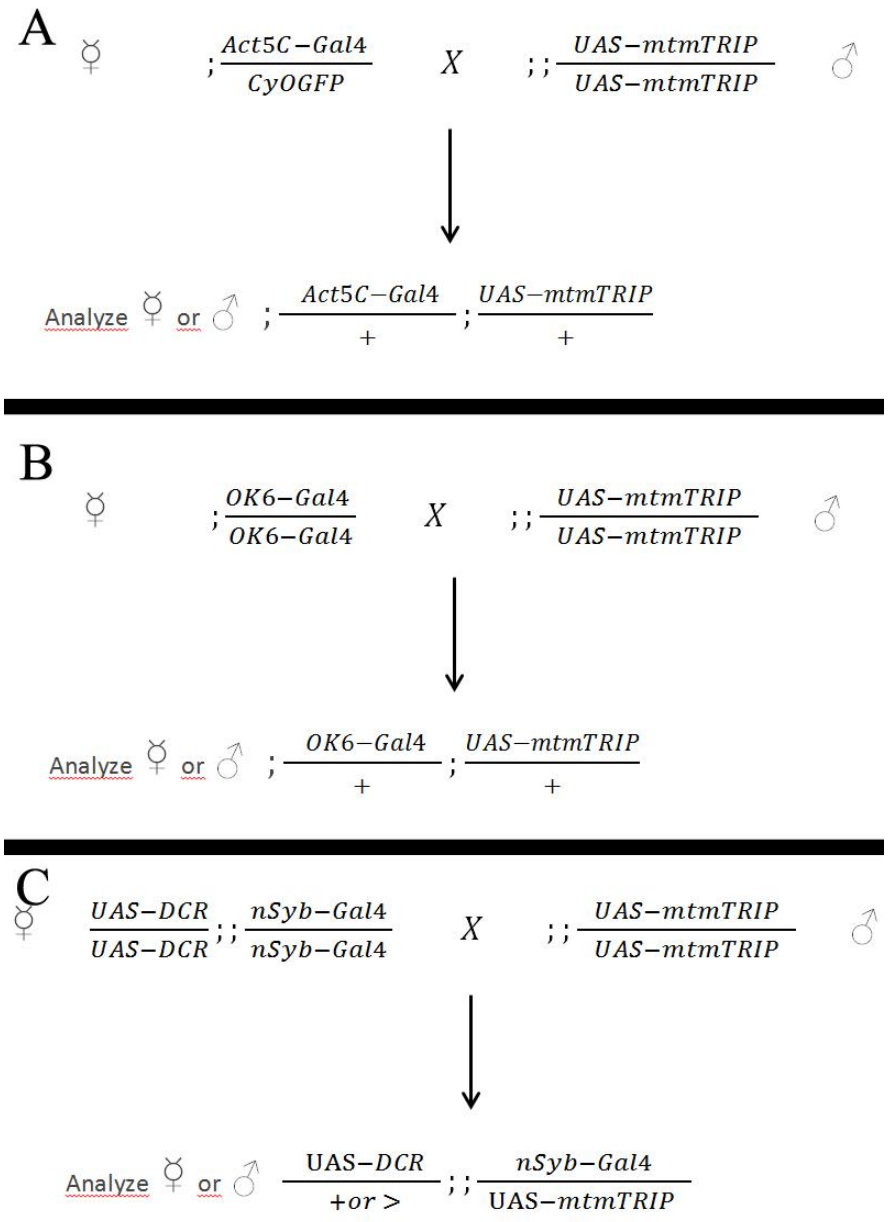

Figure 4.2. Crossing scheme for tissue specific down-regulation of *mtm* by RNAi. Mtm was down-regulated ubiquitously (A), in motor neurons (B), and in synaptic boutons (C).

The male flies were also crossed with virgin *hs:Flp, hs:ISce-I* flies, in order to mobilize the vector within the genome and target mtm *via*, homologous recombination. The crosses were transferred to new vials every third day, and at the stage of the second instar larvae they were left at 38ºC for 1 hour for heat shock to activate the flippase and further recombination.

5. RESULTS

Mutations in the myotubularin gene lead to CMT4B1 phenotype in sensory neurons although it is a ubiquitously expressed gene. The aim of this study was to investigate the function of Myotubularin in order to uncover the mechanism of how it causes CMT. We chose *Drosophila melanogaster* to investigate if mutations in myotubularin cause CMT-like phenotypes and if flies can be used as a model to study CMT pathology. In particular, we chose to study the role of mtm in NMJ establishment.

Myotubularin is a conserved protein between *Drosophila melanogaster* and *Homo sapiens*. In particular, all functional domains known to be conserved (Kerk and Moorhead, 2010). The BLAST alignment at the amino acid levels revealed a high homology with 60% identity and 77% similarity (Altshul *et al.*, 1997)

5.1. Analysis of the NMJs of *mtm*-Null Mutants

mtm-null mutant flies were generated by Velichkova and co-workers to study the mtm function for cell remodeling in animal development, and they kindly provided us with the stocks (Velichkova *et al*., 2010). In order to study the mtm function, Drosophila NMJ was chosen as a candidate neuronal structure to manifest the pathophysiological features of the peripheral CMT. As *mtm*-null flies exhibited larval lethality, techniques utilizing the third instar larvae were used.

Neuromuscular junctions (NMJs) are the synapses where a motor neuron connects to the target muscle cell. *Drosophila* NMJs are formed in the late embryonic stage and undergo a robust expansion during the larval development. The surface of the presynaptic terminals increases their size up to 10-fold, and that of the post-synaptic muscle becomes 100-fold larger in the third instar larva (Schuster *et al*., 1996). Many proteins are involved in NMJ development and proteins associated with neurodegenerative diseases were shown to affect the NMJ morphology (Bayat *et al*., 2011).

The NMJ-related experiments that were performed were immunohistochemistry and FM 1-43 dye uptake assays. Ventral muscles of the third instar larvae were used to perform NMJ-assays. *Drosophila* larvae have two large longitudinal muscles, muscle 6 and 7 and next to them, two other longitudinal ones, muscle 12 and 13, on their ventral side (Figure 5.1). The shape of NMJ on each muscle group is different. In order to obtain consistent results, NMJs innervating muscle 6 and 7 in the segment A2 were chosen for immunohistochemistry experiments and analysis was performedd using the same NMJ type. FM 1-43 dye uptake assay was performed with any NMJ type found in muscle 6-7 or 12-23.

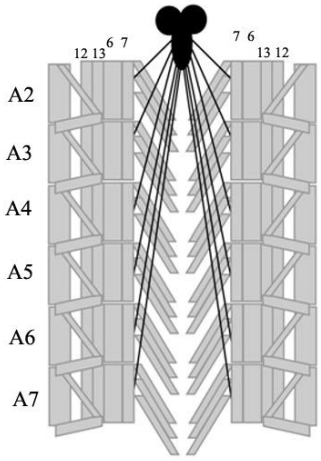

Figure 5.1. Ventral muscles of *Drosophila* larva (from Imlach and McCabe, 2009).

5.1.1. *mtm*-Null Mutants Revealed Satellite Boutons in NMJ of Third Instar *Drosophila* Larvae.

The size of NMJs increase as a larva develops, and form spherical structures, called boutons, where the neuron-muscle interaction occurs. A nerve protruding from the ventral nerve cord innervates a muscle group, like muscle 6 and 7, in each segment. The size and the shape of the NMJs on each muscle group have their own characteristics.

As mtm was speculated to have a role in peripheral neurons, its deficiency might affect the NMJ morphology. In order to determine how null mutants affect the NMJ morphology at the third instar stage immunohistochemistry experiments were performed.

For this purpose, the NMJ found on the muscles 6-7 in the segment A2 were analyzed, since it is one of the longest NMJs in the larva.

In this study, *mtm*-null larvae were used. The mutant alleles were generated by P-element excision, and 77 and 210 amino acids were deleted nearby the *P*-element entry site (Figure 5.2) (Velichkova *et al.*, 2010). N-terminal part of *mtm* was deleted in each allele, and it resulted in null phenotype showing larval lethality. Additionally, an allele which carries a point mutation in the catalytic motif also showed larval lethality due to the loss of mtm activity. The homozygous mutant and the compound heterozygous mutant larvae exhibited the same phenotype. As these alleles might have any polymorphisms in their sequence, the compound heterozygous larvae were used in this study in order to eliminate effects of possible polymorphisms.

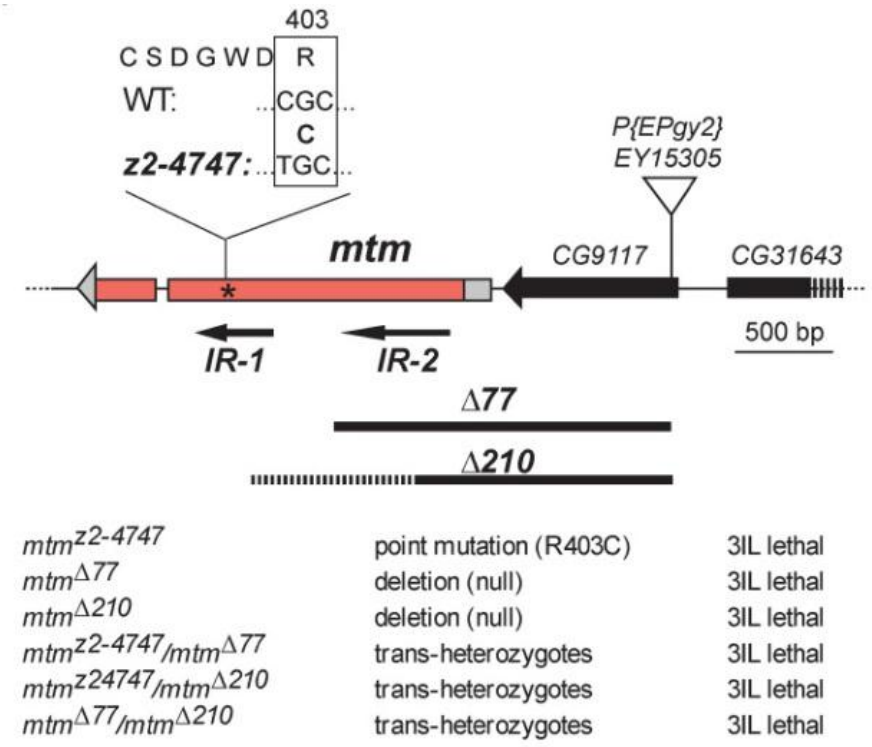

Figure 5.2. Larval lethal *mtm* mutant alleles (from Velichkova *et al*., 2010).

Anti-HRP and anti-DLG markers were used to stain the neuronal membrane and the post-synaptic areas, respectively. The compound heterozygous mutants for the null and point mutation alleles ($mtm^{\Delta 77}/mtm^{\Delta 210}$, $mtm^{\Delta 77}/mtm^{z2\text{-}4747}$ and $mtm^{\Delta 210}/mtm^{z2\text{-}4747}$) exhibited

satellite boutons in their NMJ, whereas the boutons of control larvae, w^{1118}, had a round shape (Figure 5.3, Figure 5.4, Figure 5.5 and Figure 5.6).

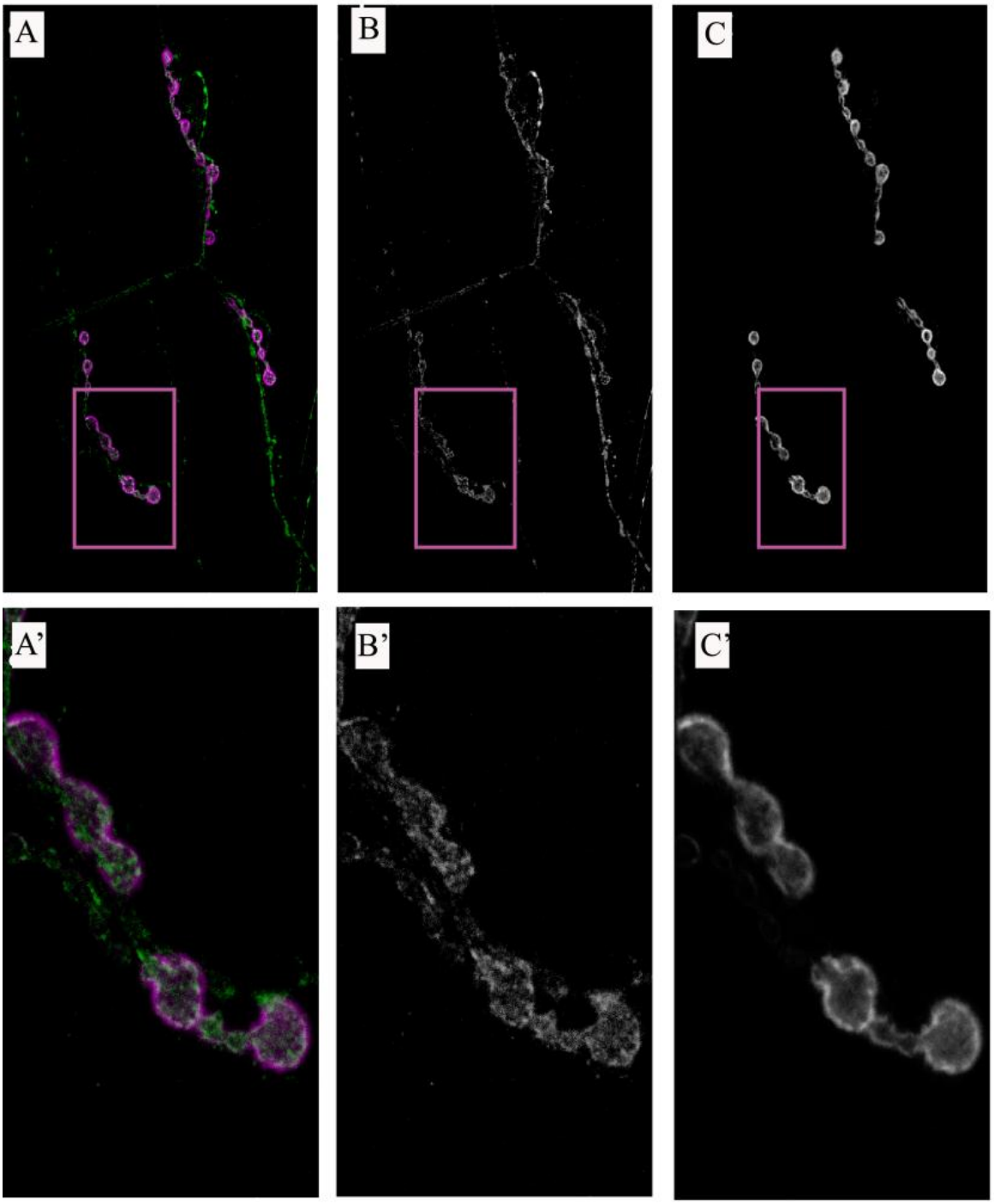

Figure 5.3. Morphology of NMJ of wild type third instar larvae in the segment A2. (A) is the merged image of anti-HRP (green) (B) and anti-DLG (magenta) (C) stainings. The images at the bottom show the 4X magnification of the indicated boutons (A', B' and C'). Anti-HRP stains the neuronal membrane and anti-DLG stains the post-synaptic area.

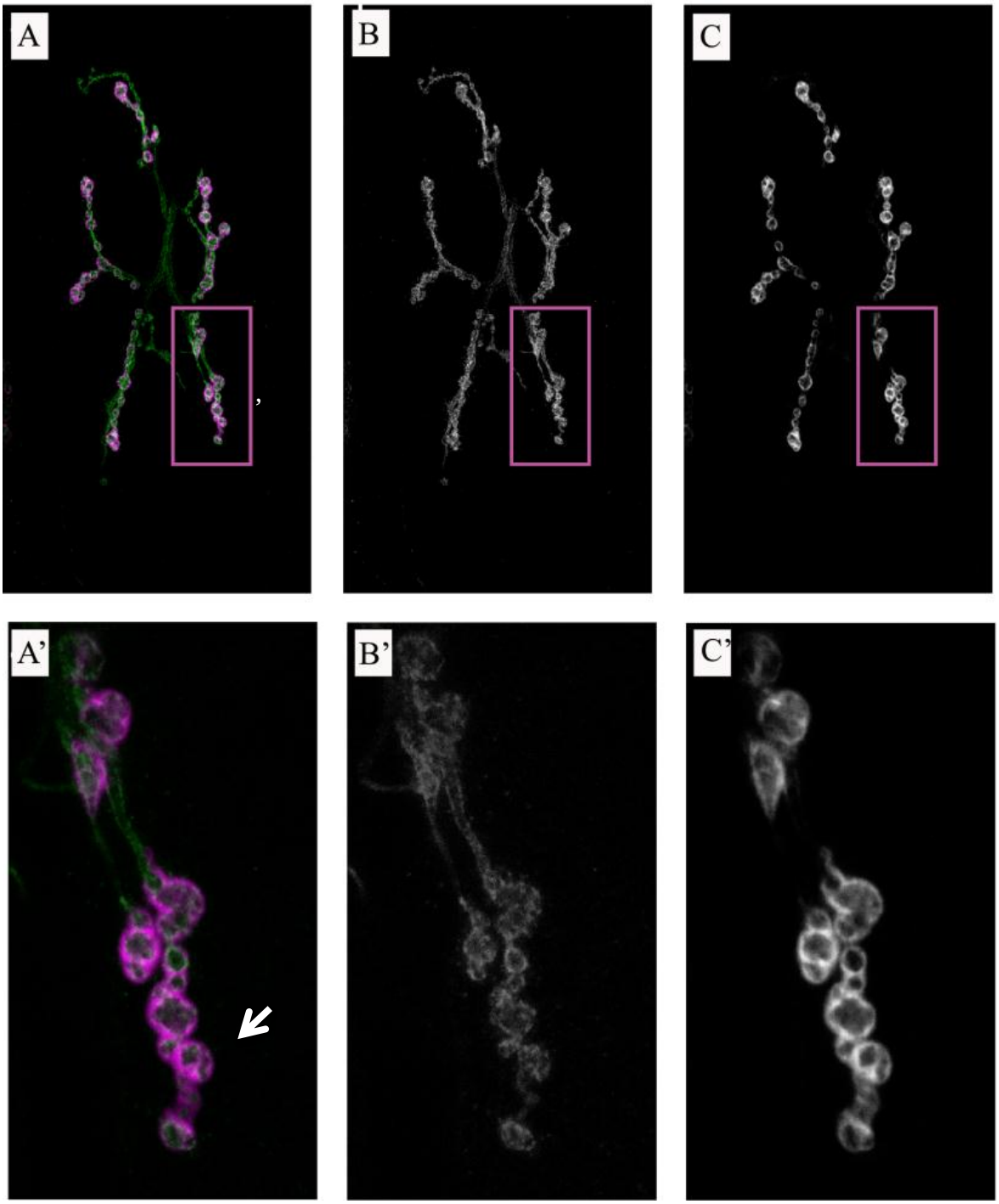

Figure 5.4. Morphology of NMJ of *mtm*$^{\Delta 77}$/*mtm*$^{\Delta 210}$ larva in the segment A2. (A) is the merged image of anti-HRP (green) (B) and anti-DLG (magenta) (C) stainings. The images at the bottom show the 4X magnification of the indicated boutons (A', B' and C'). Mutant larva exhibited satellite boutons all over the NMJ (arrow).

mtm$^{\Delta 77}$/*mtm*$^{\Delta 210}$ larva were also double-stained by anti-CSP and anti-HRP antibodies. As anti-HRP stains the neuronal membrane, anti-CSP labels synaptic vesicles (close to T-bar ribbon). The mutant larva revealed an abnormal synaptic bouton structure (Figure 5.7).

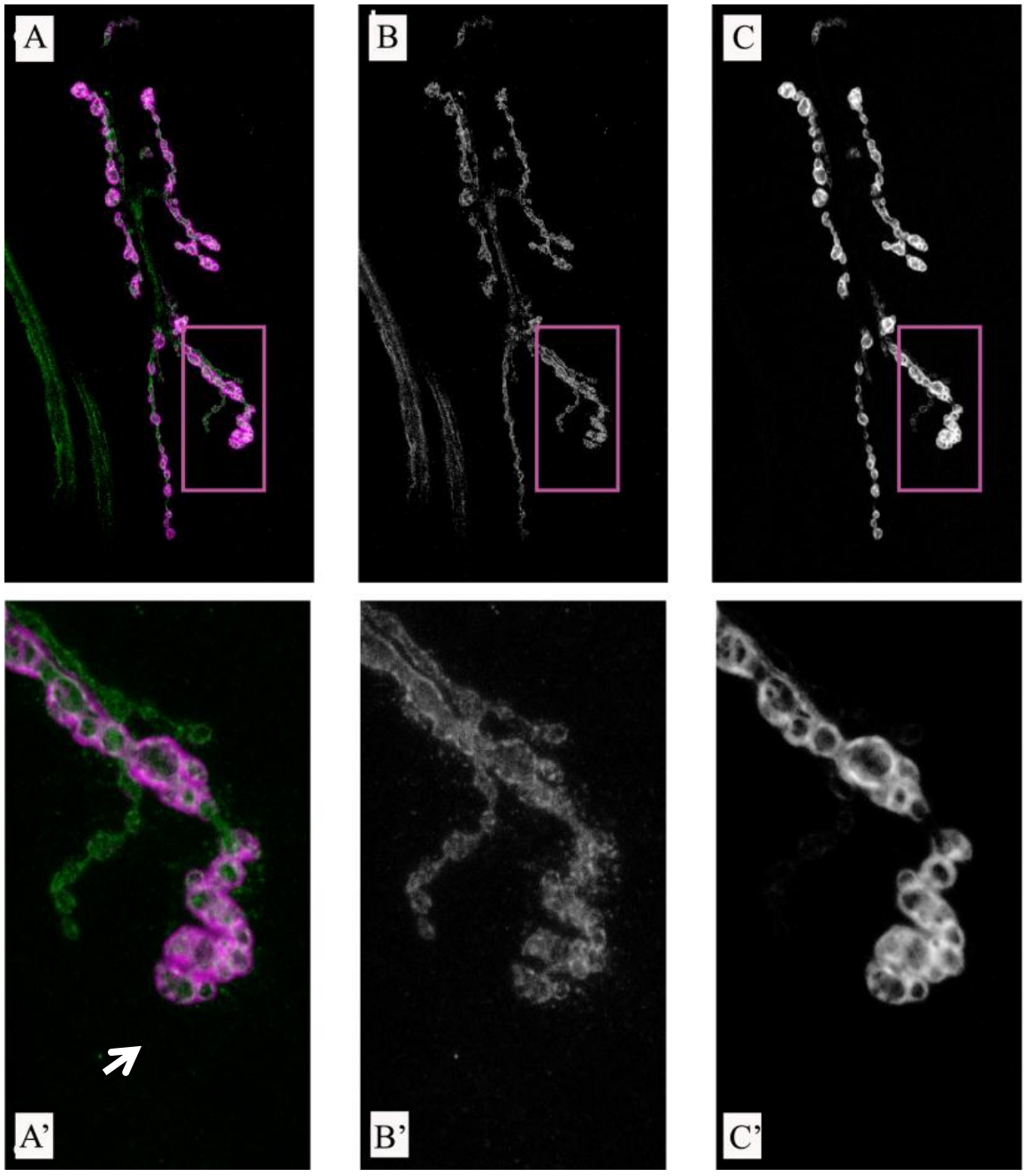

Figure 5.5. Morphology of NMJ of *mtm*$^{\Delta 77}$/*mtm*$^{z2\text{-}4747}$ larva in the segment A2. (A) is the merged image of anti-HRP (green) (B) and anti-DLG (magenta) (C) stainings. The images at the bottom show the 4X magnification of the indicated boutons (A', B' and C'). Mutant larva exhibited satellite boutons in the NMJ (arrow).

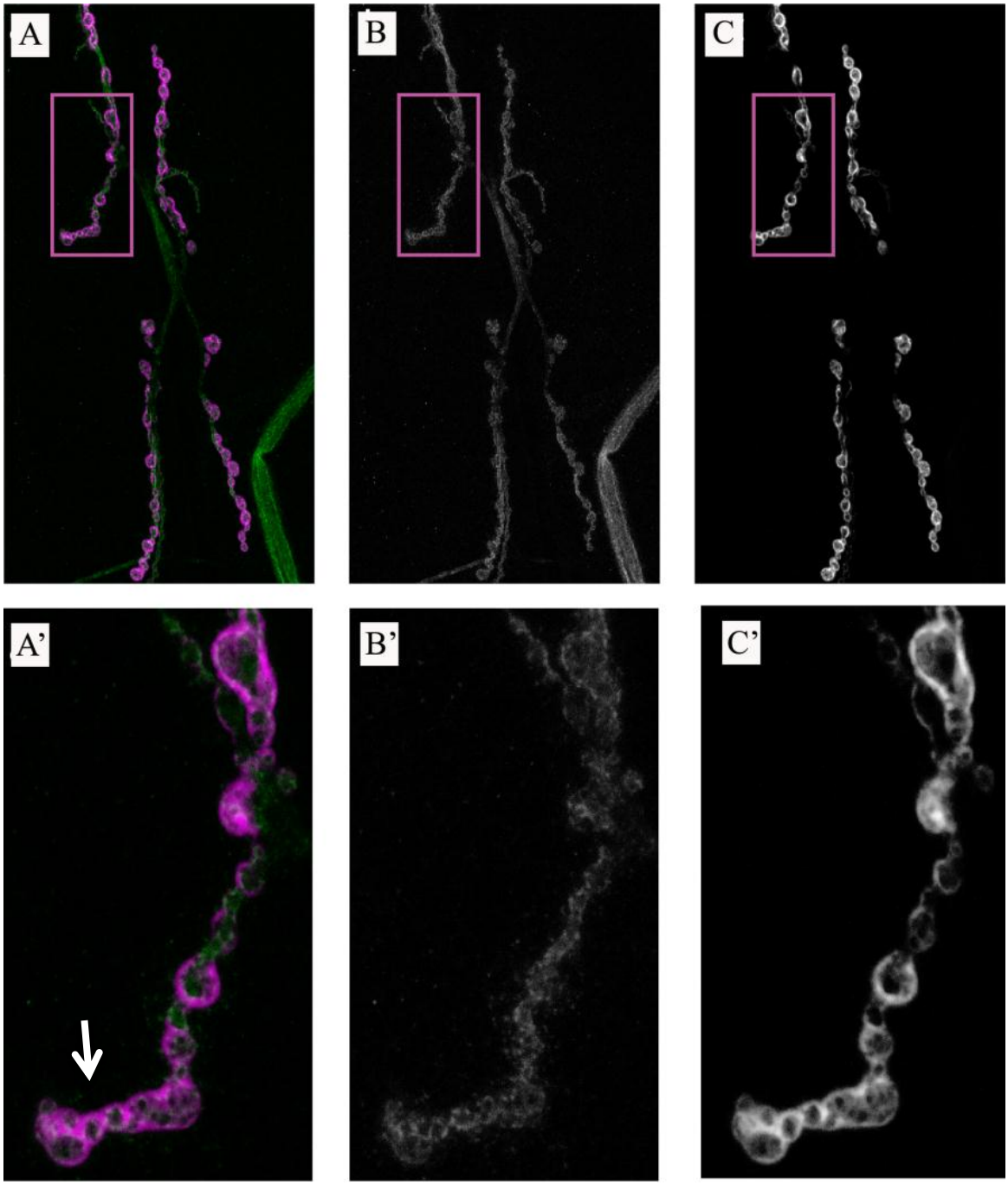

Figure 5.6. Morphology of NMJ of *mtm*$^{\Delta 210}$/*mtm*$^{z2\text{-}4747}$ larva in the segment A2. (A) is the merged image of anti-HRP (green) (B) and anti-DLG (magenta) (C) stainings. The images at the bottom show the 4X magnification of the indicated boutons (A', B' and C'). Mutant larva exhibited satellite boutons (arrow).

The NMJ of *mtm*$^{\Delta 77}$/*mtm*$^{\Delta 210}$ larva were also double-stained by anti-Synorf1 and anti-HRP antibodies. Anti-Synorf1 labels synapsin protein, which is found predominantly in the presynaptic area, it has a role in neurotransmitter release (Figure 5.8).

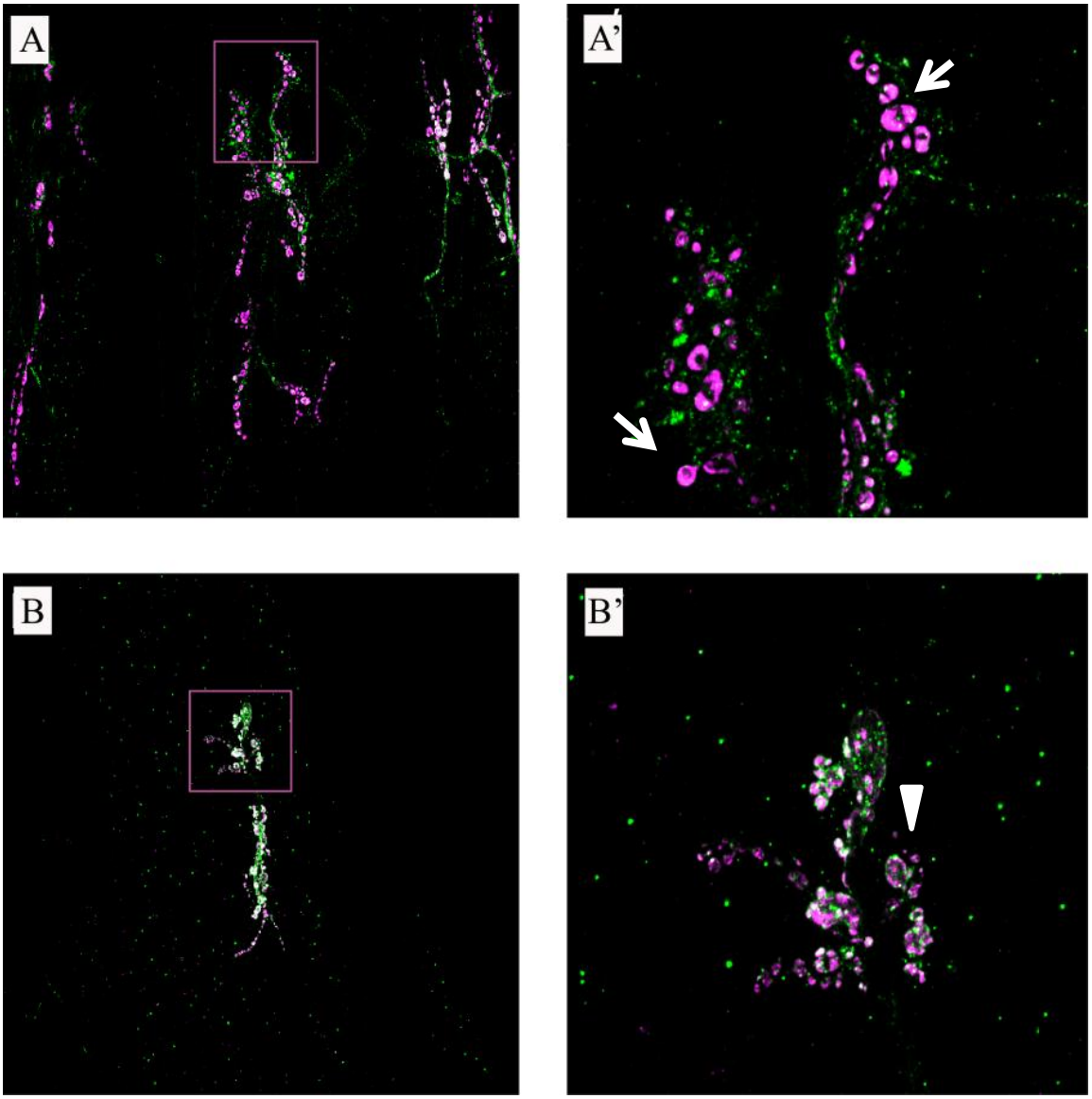

Figure 5.7. Morphology of NMJ of $mtm^{\Delta 77}/mtm^{\Delta 210}$ larva stained with anti-CSP (magenta) and anti-HRP (green). (A) is the control larva, w^{1118}, and (B) is the $mtm^{\Delta 77}/mtm^{\Delta 210}$ larva. (A') and (B') show the 4X magnified boutons of the indicated area of corresponding NMJ. Control larva showed spherical boutons (arrows). Mutant larva showed abnormal distorted boutons without firm spherical shape (arrowhead).

Pre- and post-synaptic antibodies were used to study the NMJ morphology, and it was observed that the compound heterozygous mutant larvae show abnormal NMJ structures with satellite boutons and distortion in the spherical shape of the overall NMJ boutons. Thus, lack of mtm seems to have a clear effect on the NMJ structure. Additionally, the ratio of the length of the NMJs to the muscle area was measured using

ImageJ. 19 mutant and 17 control larvae was analyzed and the length of the NMJ did not differ significantly between the mutants and the control (Figure 5.9).

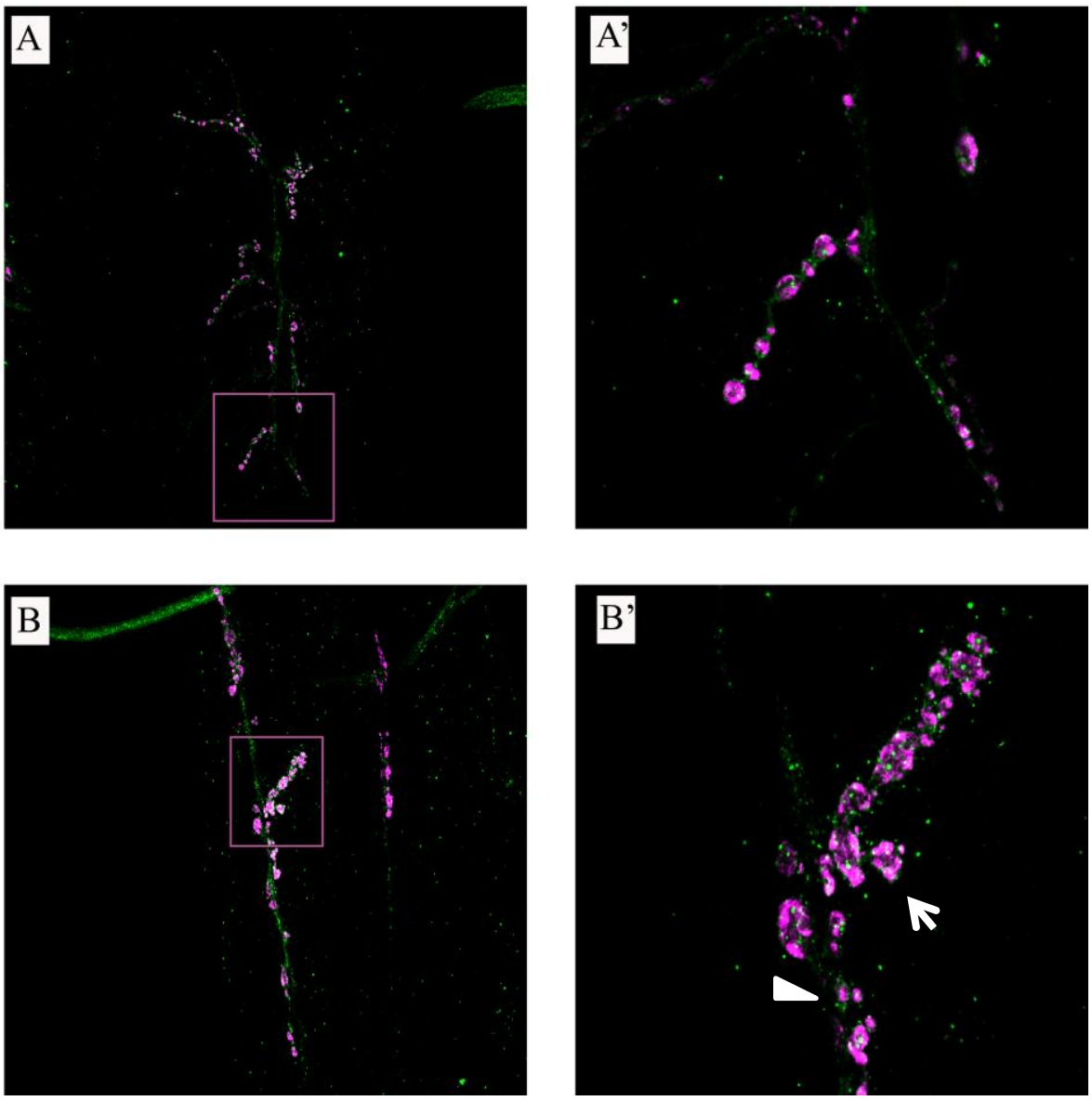

Figure 5.8. Morphology of NMJ of $mtm^{\Delta 77}/mtm^{\Delta 210}$ larva stained with anti-Synorf1 (magenta) and anti-HRP (green). (A) is the control larva, w^{1118}, and (B) is the $mtm^{\Delta 77}/mtm^{\Delta 210}$ larva. (A') and (B') show the 4X magnified boutons of the indicated area of corresponding NMJ. Control larva showed spherical boutons. Mutant larva showed abnormal boutons (arrow) exhibiting satellite boutons and distorted shape (arrowhead).

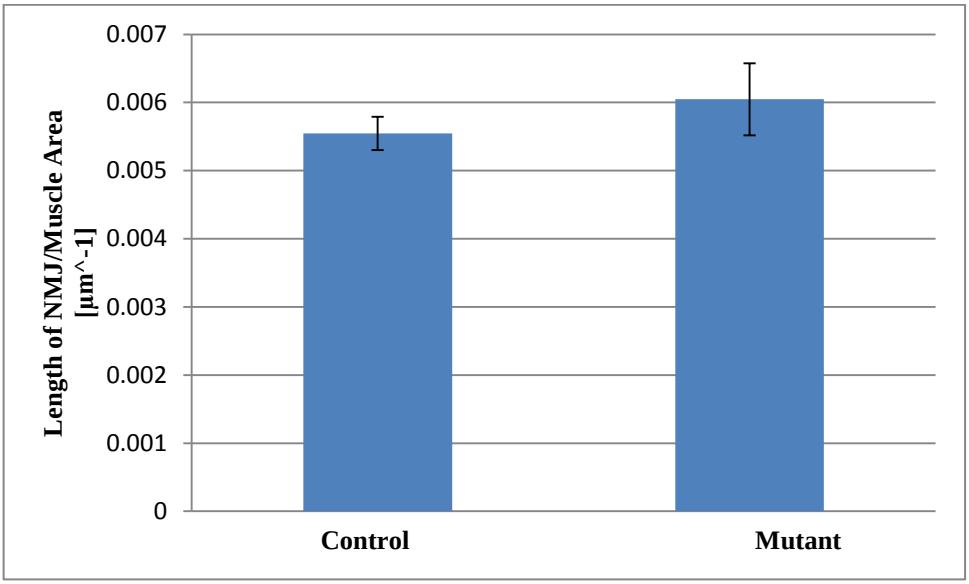

Figure 5.9. The ratio of the length of the NMJs to the innervated muscle area. The error bars show the standard error of mean (P-value for two-tailed t-test = 0.3775).

5.1.2. FM 1-43 Dye Uptake Assay

FM 1-43 (N-(3-triethylammoniumpropyl)-4-(4-(dibutylamino)styril)pyrimidinium dibromide) dye is used for the assessment of the vesicle recycling at the terminal boutons (Verstreken *et al.*, 2008). FM 1-43 is a nonfluorescent dye in aqueous medium, but it fluoresces when bound to its target membrane phospholipids. Live tissue samples are treated with FM 1-43 dye, and stimulated. The level of fluorescence is used to measure the neurotransmitter re-uptake by endocytosis (Betz and Bewick, 1992).

FM 1-43 dye uptake assays were performed with compound heterozygous mutant larvae. Alive larvae were treated with fluorescent FM 1-43 dye in stimulation solution with 90 mM KCl. The chemically excited synapses internalized the dye by endocytosis and the stimulation was interrupted using standard low K^+-ion containing HL-3 solution. The not-internalized dye was washed away and the fluorescent images were taken by a Nikon FN1 microscope and the light was filtered through a FITC filter. The bouton structure and level of fluorescence was assessed using Amira 2.2 software.

The analysis showed that boutons of mutant and control larvae displayed different morphology. While the control larvae exhibited spherical and smooth boutons, satellite boutons and submembrane inclusions were observed in the mutant larvae (Figure 5.10).

The quantitative analysis was performed using Amira 2.2 software. The level of fluorescence was measured for 8 larvae for the mutants and the larvae, and the average fluorescence intensity of mutant and the control larvae were compared. The level of fluorescence was not significantly different between control and the mutants (P-value for two-tailed t-test = 0.3245) (Figure 5.11).

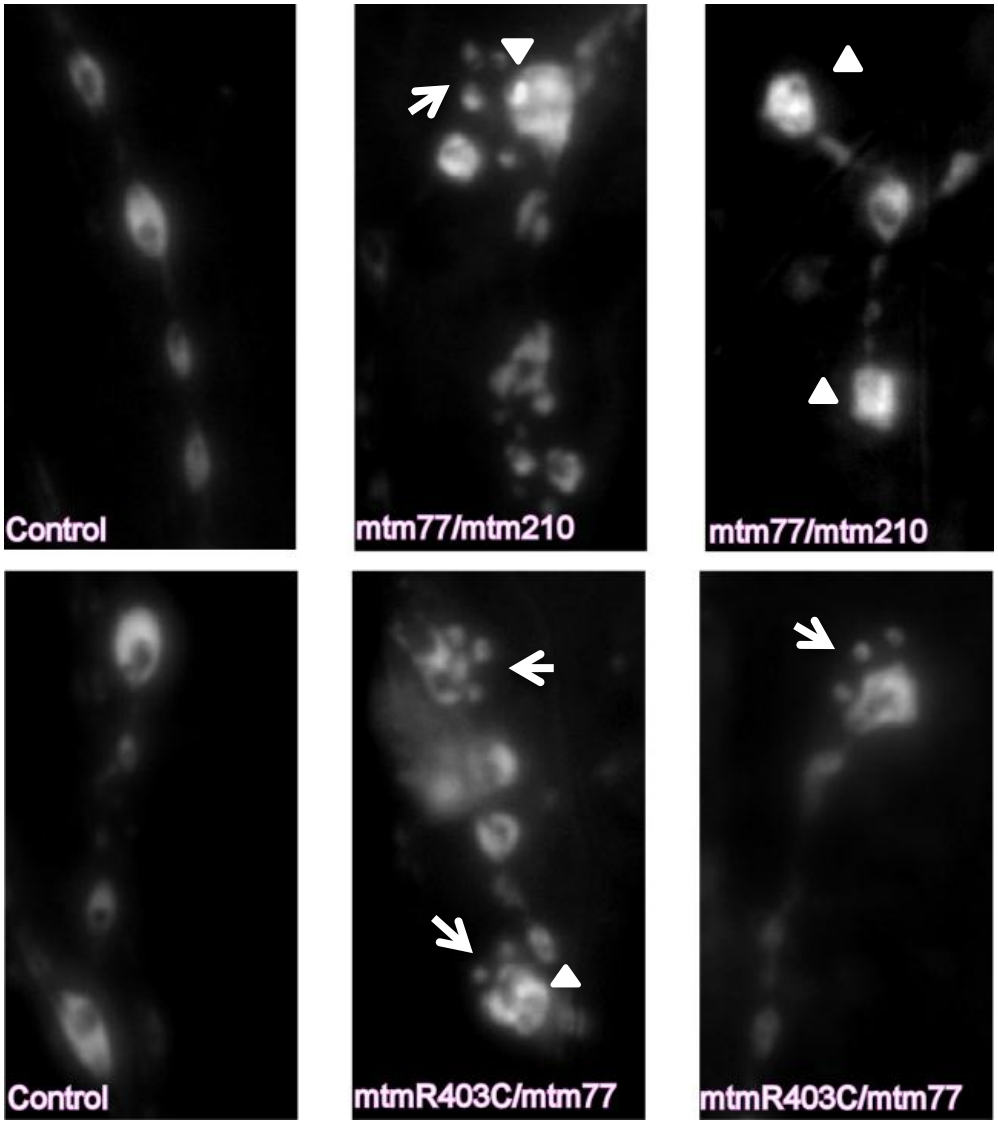

Figure 5.10. FM 1-43 Dye uptake assay. Mutant larvae revealed satellite boutons (arrow) and submembrane inclusions (arrowhead).

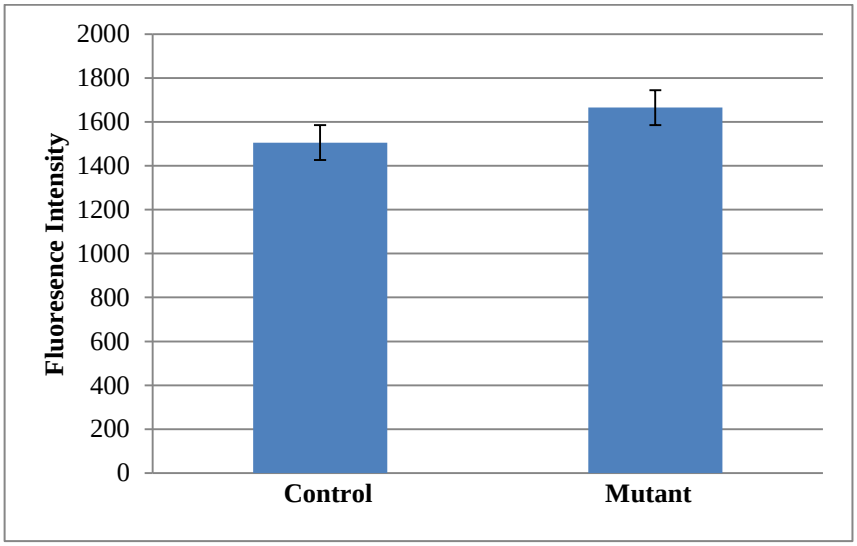

Figure 5.11. The average level of fluorescence intensity of the control and the mutant larvae in FM 1-43 dye uptake assay. The error bars indicate the standard error of mean (P-value for two-tailed t-test = 0.3245).

To summarize, the loss of mtm function in flies has an effect on NMJ morphology. The results of immunohistochemistry experiments to reveal the morphology of the NMJ and FM 1-43 dye uptake experiments to test its functionality were consistent; both revealed abnormal NMJ morphology with defects in bouton shape, an increase in satellite bouton structure and the presence of detectable submembrane inclusions.

5.2. Analysis of RNAi Lines

In order to analyze the effect of down-regulation of *mtm* in different tissues, an already established mtm-TRIP RNAi line was used. The double-stranded RNA sequence of *mtm* was expressed ubiquitously, in motor neurons, and in the presynaptic area using actin5C-GAL4, OK6-GAL4 and n-Syb-Gal4 driver lines, respectively.

Expression of mtm RNAi using the actin5C-driver resulted in pupal lethality. Keeping the crosses at 29ºC, only 33% of the progeny carrying mtmTRIP RNAi could enter the pupal phase, and no adult flies were observed. As the *mtm*-null mutants cannot enter the adult phase, it can be speculated that ubiquitous down-regulation of mtm by RNAi has a similar on longevity of the flies. OK6-GAL4 crosses were also kept at 29 ºC to express GAL4 protein.

n-Syb-GAL4 driver was used together with a UAS-Dicer allele. Dicer is a protein which increases the efficiency of cellular RNAi mechanisms. Using n-Syb-GAL4 driver only to down-regulate *mtm* did not result in any significant morphologic effect; therefore this driver was used along with UAS-Dicer responder. To increase the down-regulation effect in synapses this cross was kept at 25 ºC, since Dicer activity has side effects for synapses, when the crosses were kept at 29 ºC.

The progeny larvae, expressing *mtm*-RNAi selectively, were collected from each cross as described in Figure 4.2 and were immunostained to visualize the NMJ morphology. The ubiquitousdown-regulation of *mtm* using actin5C-driver resulted in similar boutons in the NMJs as the control, but at the very end of the NMJs they showed satellite boutons (Figure 5.12). The down-regulation of *mtm* using OK6- for down-regulation in neurons and n-Syb-drivers for down-regulation in the presynaptic are also resulted in the same phenotypes; satellite boutons were only found at the ends of the NMJ branches (Figure 5.13 and 5.14).

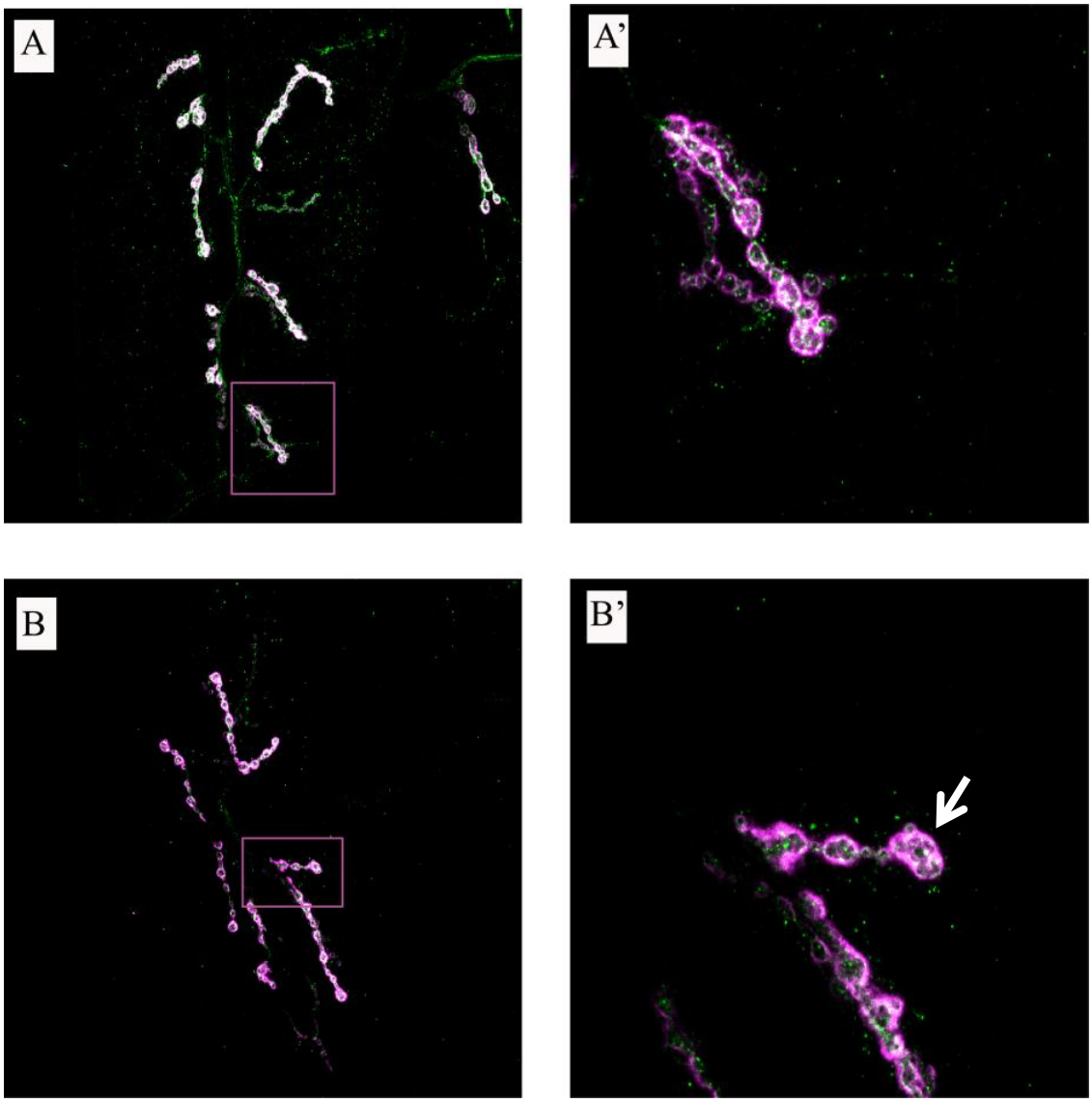

Figure 5.12. Morphology of NMJ actin5C→UAS-mtmTRIP lines. Larvae were stained with anti-DLG (magenta) and anti-HRP (green). (A) is the control larva, actin5C-GAL4 in yv background, and (B) is the actin5C→UAS-mtmTRIP larva. (A') and (A') show the 4X magnified boutons of selected area. Control larva showed spherical boutons, yet, some satellite boutons were observed in the actin5C→UAS-mtmTRIP larva (arrow).

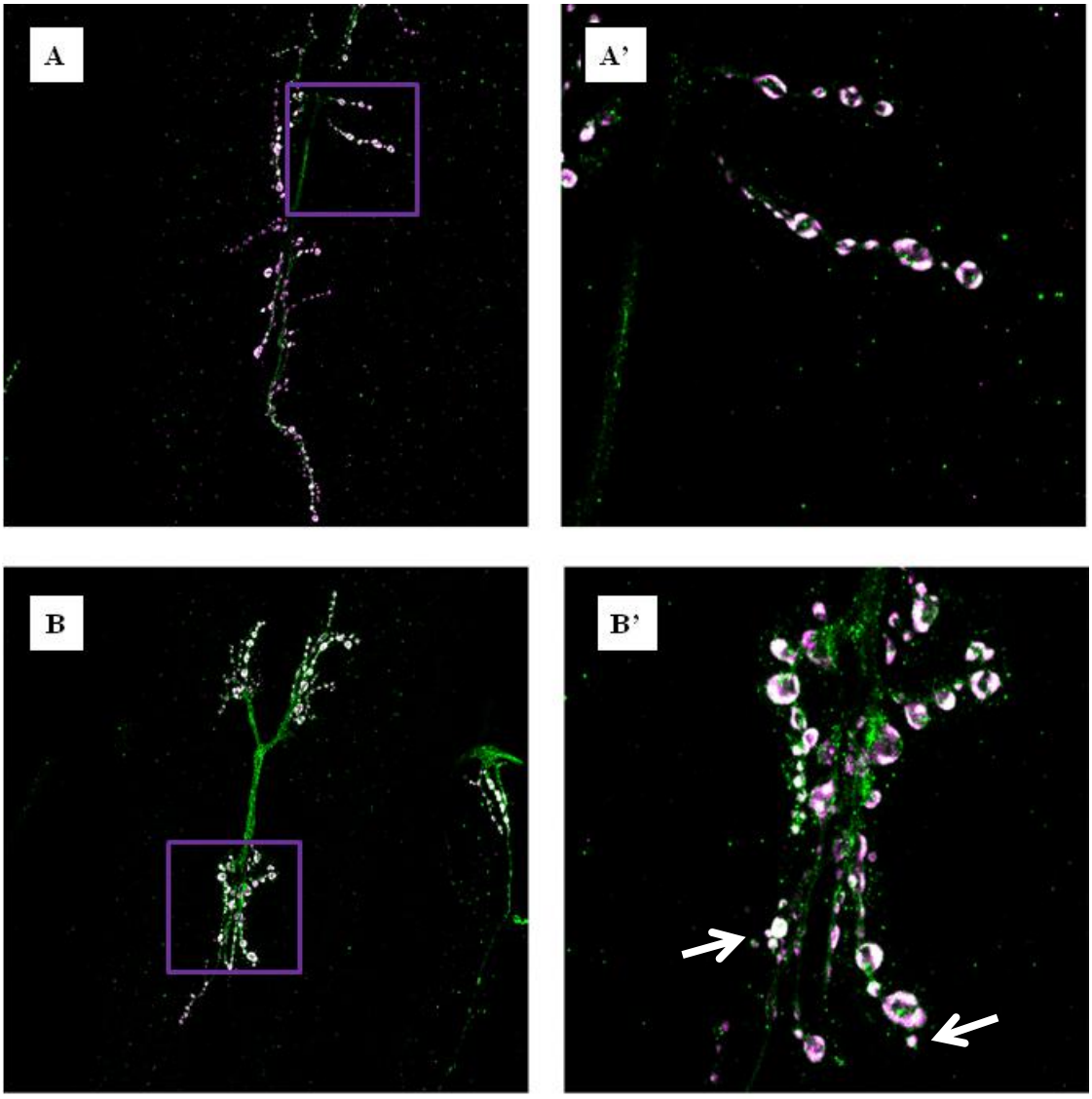

Figure 5.13. Morphology of NMJ actin5C→UAS-mtmTRIP lines. Larvae were stained with anti-CSP (magenta) and anti-HRP (green). (A) is the control larva, actin5C-GAL4 in yv background, and (B) is the actin5C→UAS-mtmTRIP larva. (A') and (A') show the 4X magnified boutons of the selected area. Control larva showed spherical boutons, satellite boutons were observed in the actin5C→UAS-mtmTRIP larva (arrow).

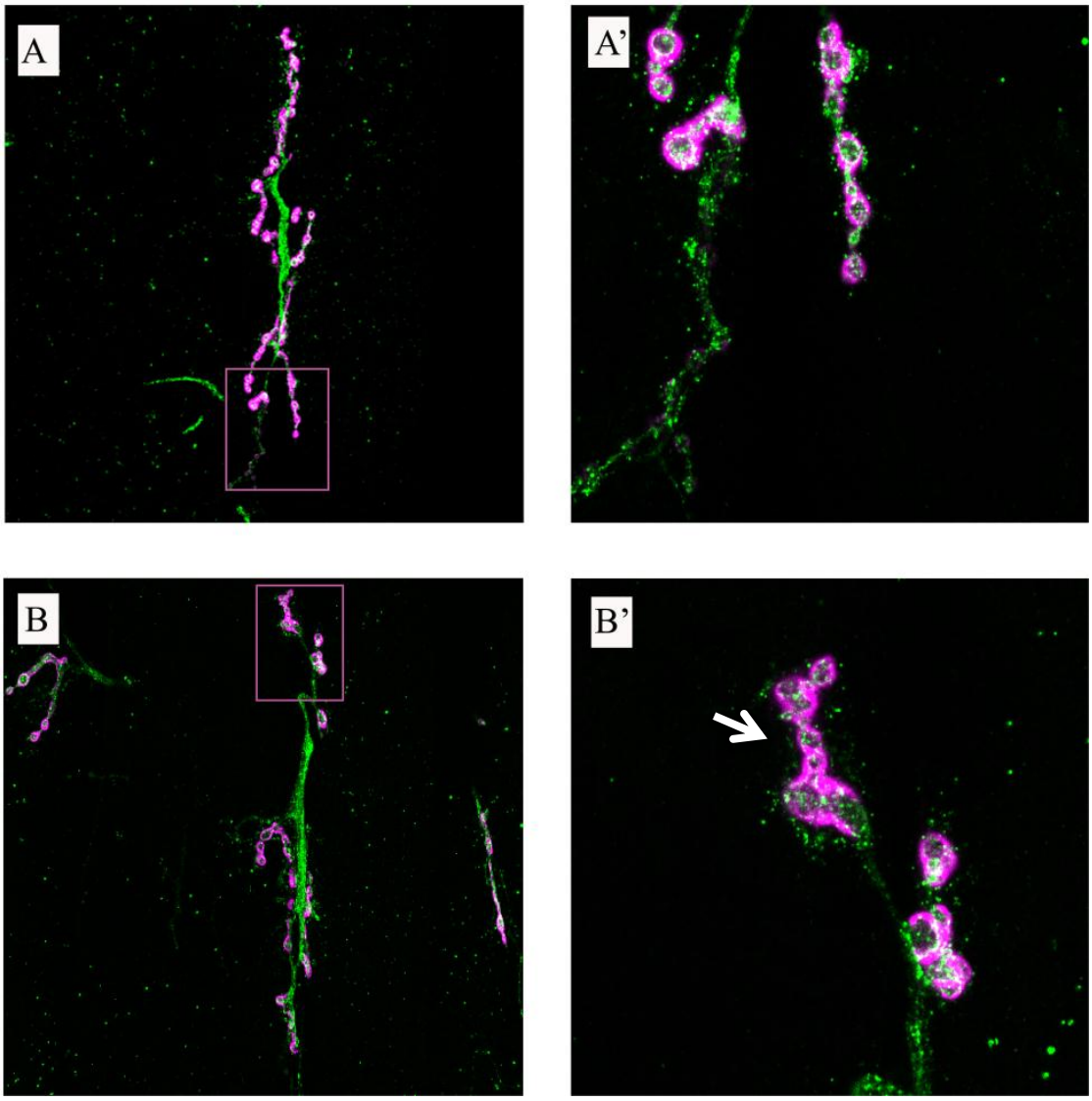

Figure 5.14. Morphology of NMJ OK6-GAL4→UAS-mtmTRIP lines. Larva were stained with anti-DLG (magenta) and anti-HRP (green). (A) is the control larva, OK6-GAL4 in yv background, and (B) is the OK6-GAL4→UAS-mtmTRIP larva. (A') and (B') show the 4X magnified boutons of the indicated area of corresponding NMJ.

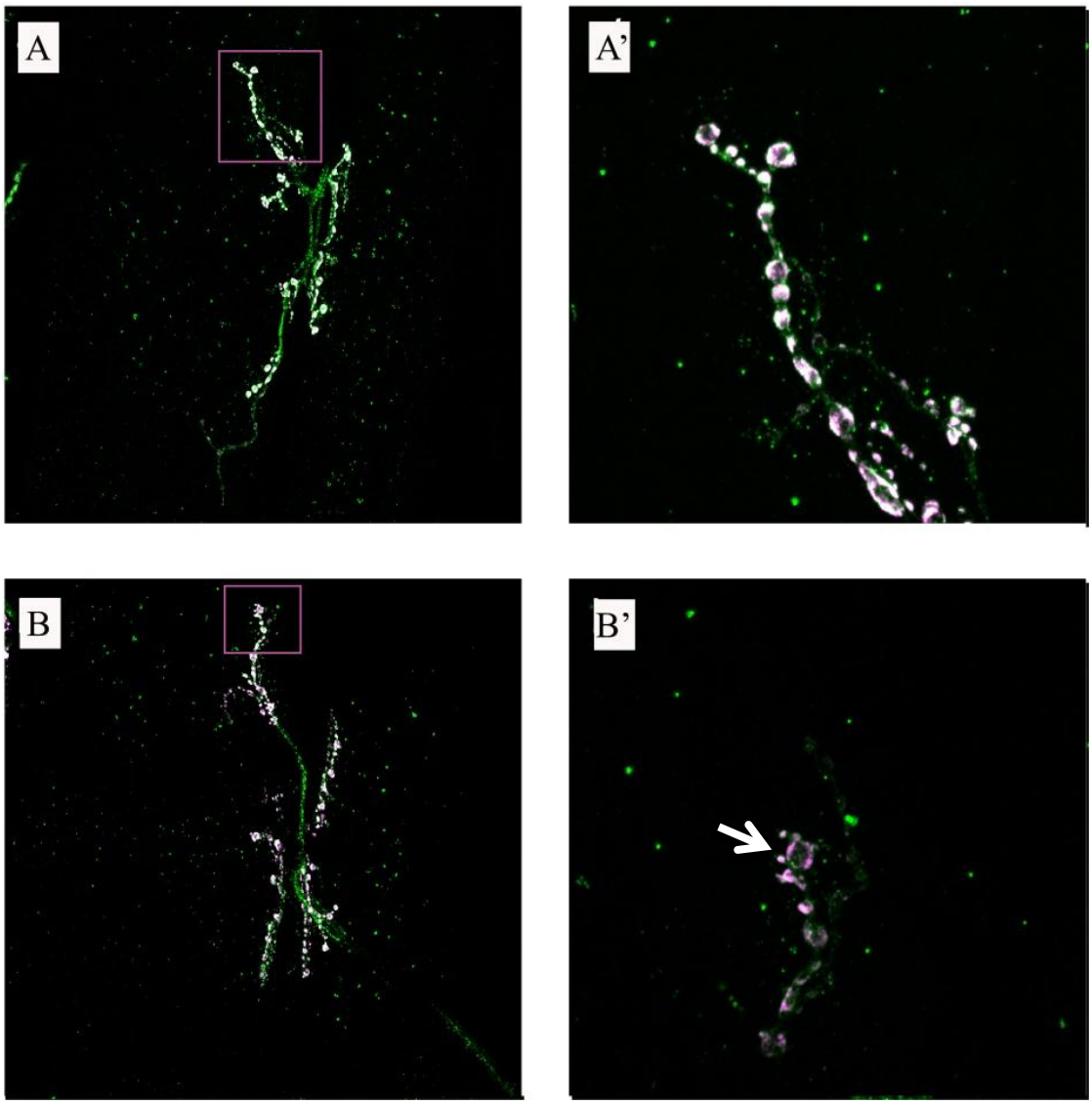

Figure 5.15. Morphology of NMJ n-Syb-GAL4→UAS-mtmTRIP, UAS-Dicer lines. Larva were stained with anti-Synorf1 (magenta) and anti-HRP (green). (A) is the control larva, n-Syb-GAL4→ UAS-Dicer in yv background, and (B) is the n-Syb-GAL4→UAS-mtmTRIP, UAS-Dicer larva. (A') and (A') show the 4X magnified boutons of the selected area. n-Syb-GAL4→UAS-mtmTRIP, UAS-Dicer larva exhibited satellite boutons (arrow).

5.3. Targeting *mtm* for Homologous Recombination

5.3.1. Generation of the Targeting Vector

In order to delete mtm gene from fly genome via homologous recombination, a targeting vector carrying the flanking homology regions of *mtm* was prepared. The targeting vector that we used was pP{white-STAR} which carries a red eye marker (white$^+$, w$^+$) in its sequence. If the vector is integrated into the fly's genome with white eye background (w$^-$), the progeny is expected to have red eyes.

pP{white-STAR} is a 7237 bp circular vector, and it carries two multiple cloning sites, so that the 5' and 3' homology sequences of the gene of interest can be inserted. In this study, a modified version with additional NheI and SacII restriction sites was used, since the intrinsic SpeI and XhoI sites were also present in the 3' homology region of *mtm* (Figure 5.16). This vector has been previously modified by Güner Kaçmaz, MS; from FLY lab.

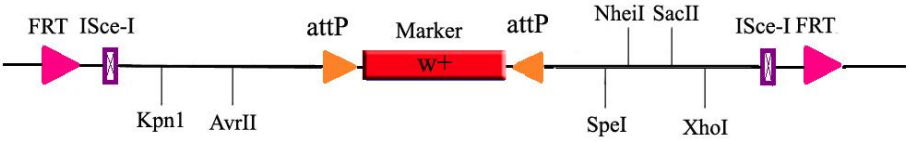

Figure 5.16. modified version of the pP{white-STAR} vector.

In addition to red eye marker w$^+$ and multiple cloning sites, pP{white-STAR} carries three important elements; *FRT* sites, ISce-I cut site and *attP* sequences. *FRT* sites facilitate the mobilization of vector in the genome upon Flippase activity. ISce-I enzyme linearizes the circular vector by cutting it on the ISce-I recognition sites. *AttP* sites flanking the marker make it a replaceable element.

Our cloning strategy comprises two fundamental steps: amplification of the flanking homology sequences of *mtm* and cloning these sequences in to pP{white-STAR}targeting vector (Figure 5.17). As SpeI, NheI and XhoI have restriction sites in the 3' homology arm, SacII recognition sites were attached to the both primer pairs to amplify this

sequence. SacII endonuclease has restriction sites in the 5’ homology arm, therefore the 5’ homology arm was cloned into pP{white-STAR} after cloning of the 3’ homology arm.

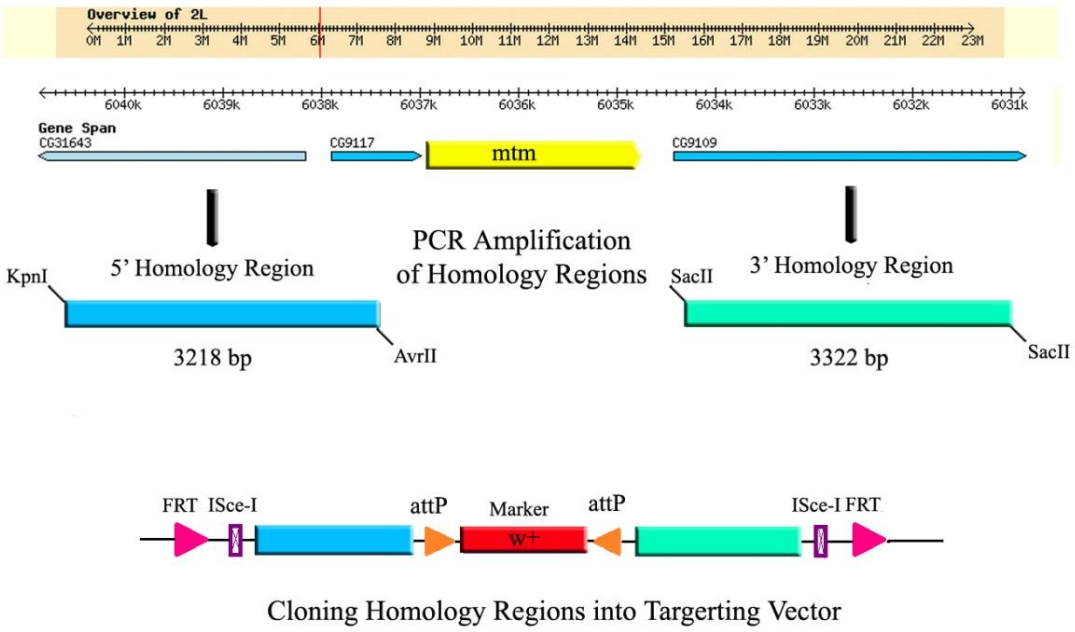

Figure 5.17. Generation of *mtm*-targeting vector.

5.3.1.1. Restriction Disgestion of BAC by NotI. The genomic BAC clone containing *mtm*, BACR10M11, was purchased and cultured as described. Five different colonies were cultured and BAC DNA was isolated. The length of the BAC is 186.5 kb and it was expected that the NotI restriction digestion result in 6 DNA fragments of 6533 bp, 8737 bp, 10314 bp, 19056 bp, 53487 bp and 88329 bp long. The DNA sequence of each BAC clone was verified by NotI restriction (Figure 5.18). The first and the fourth colony resulted in correct digestion pattern. The further experiments were done using DNA of the first colony.

5.3.1.2. Amplification of the homology sequences flanking mtm. In order to amplipy 5’ and 3’ homology sequences, primers that suitable restriction sites were designed using ApE-A Plasmid Editor v2.0.37 and care was taken to have primer pairs of close melting temperature values. 5’ and 3’ homology sequences were amplified by Phusion polymerase using BACR10M11DNA as template. To amplify the 5’ sequence the primer pair, CG9115_5HF and CG9115_5HR were used. The forward primer, CG9115_5HF, carried a KpnI recognition site at its 5’ end, whereas the reverse primer, CG9115_5HR, carried an

AvrI site. The amplification of 3’ homology sequence was done using CG9115_3HF and CG9115_3HR, as forward and reverse primers, respectively. Both primers had a SacII recognition site attached at their 5’ ends. The expected sizes of amplicons were 3226 and 3332 bp for 5’ and 3’ sequences, respectively. The high fidelity PCR yielded in expected DNA fragments (Figure 5.19). The DNA bands were excised from the gel and used for further cloning experiments.

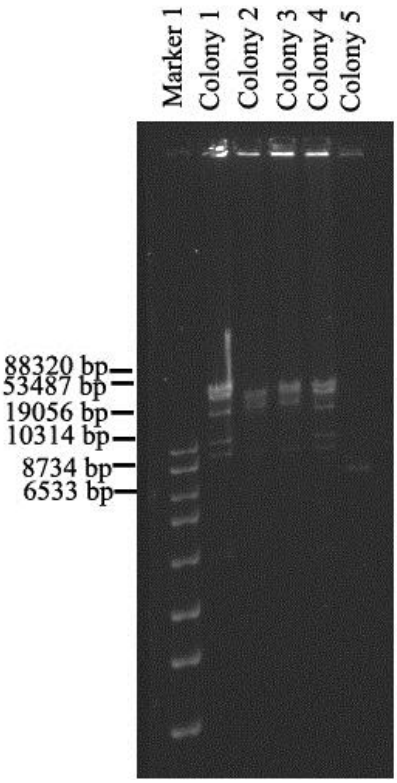

Figure 5.18. Restriction digestion of BACR10M11 by NotI restriction endonuclease. Marker 1 stands for 1kb DNA ladder (SM0311, Thermo Scientific).

5.3.1.3. Cloning Homology Sequences into pP{white-STAR}. In order to sequence the whole PCR fragments and to have their continuous production without any mutation, the PCR amplicons were subcloned into pCR-Blunt II-TOPO vector. The amplicons generated by Phusion polymerase were blunt-ended, hence the DNA fragment of 5’ and 3’ homology regions of mtm were ligated directly into pCR-BluntII-TOPO vector without any modification. The ligation products were transformed to *E. coli* cells and next day, positive colonies carriying the desired insert were screened by colony PCR (Figure 5.20). For 5’ homology arm, primer pair CG9115_5H_S4 and CG9115_5HR was used that upon

amplification produces a 949 bp DNA fragment. For 3’ homology arm, the primers CG9115_3H_S4 and CG9115_3HR were used and yielded in 1107 bp fragment. Five positive colonies were chosen for each fragment (Colonies 1,4,8,11 and 17 for 5’ homology arm and Colonies 1,3,7,10 and 18). The picked colonies were grown in liquid medium and plasmids were isolated. Their sequences were determined by Sanger sequencing (Macrogen, Korea), and luckily none of them carried mutations.

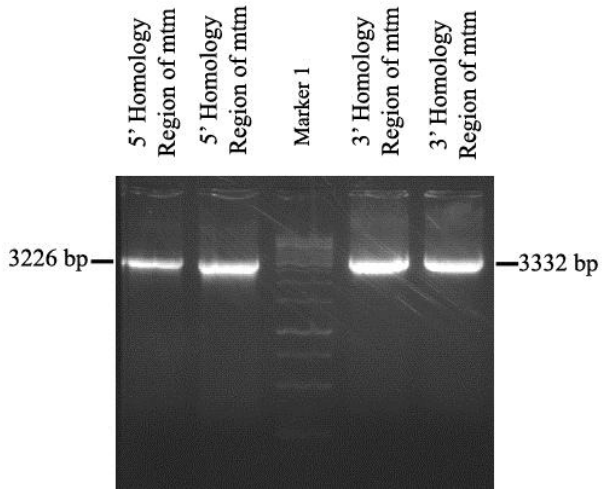

Figure 5.19. Amplification of 5’ and 3’ homology sequences flanking *mtm.* Marker 1 stands for 1kb DNA ladder (SM0311, Thermo Scientific).

After verifying that the inserts do not carry any mutations, the construct carrying 5’ homology arm was digested by KpnI and AvrII, and the construct carrying 3’ homology arm was digested with SacII (Figure 5.21). The restriction fragments run on agarose gel were 3220 and 3326 bp long respectively, and were extracted from the gel.

As SacII has a restriction site in the 5’ homology arm, the first fragment inserted into the vector was the 3’homology arm. The vector pP{white-STAR}was digested with SacII and the 3’ homology arm was ligate. The orientation of the fragment was checked by NheI digestion pattern. The expected bands of the correct orientation were 573 and 10010 bp, and six colonies showed the correct pattern on the gel (Figure 5.22a).

5’ homology arm was inserted into the generated construct carrying the 3’ homology arm. The vector was cut by KpnI and AvrII, and 5’ homology arm was inserted. Bacteria

are transformed and the construct was isolated. The final construct was checked through NheI and SacII digestion, and its digestion pattern was confirmed (Figure 5.22b).

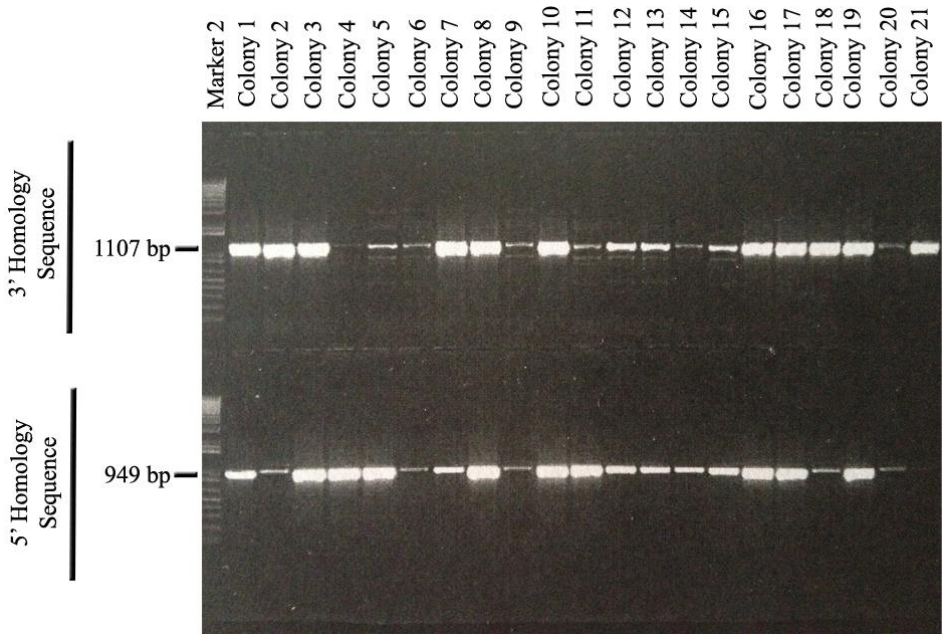

Figure 5.20. Verification of cloning Homology arms flanking mtm into pCR-Blunt II-TOPO *via* colony PCR. Marker 2 stands for 1kb plus DNA ladder (10787-018, Life Technologies).

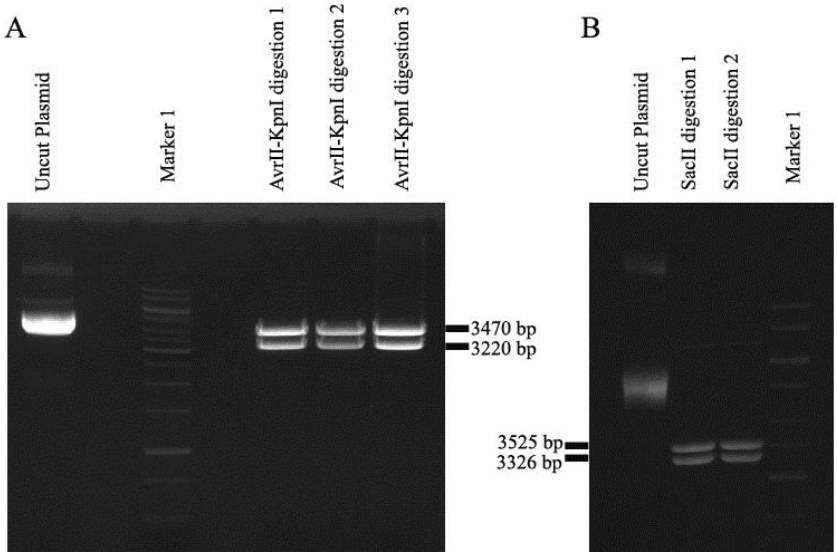

Figure 5.21. Restriction digestion of pCR-Blunt II-TOPO constructs of homology arms. (A) 5' homology arm - pCR-Blunt II-TOPO. (B) 3' homology arm - pCR-Blunt II-TOPO. 1 stands for 1kb DNA ladder (SM0311, Thermo Scientific).

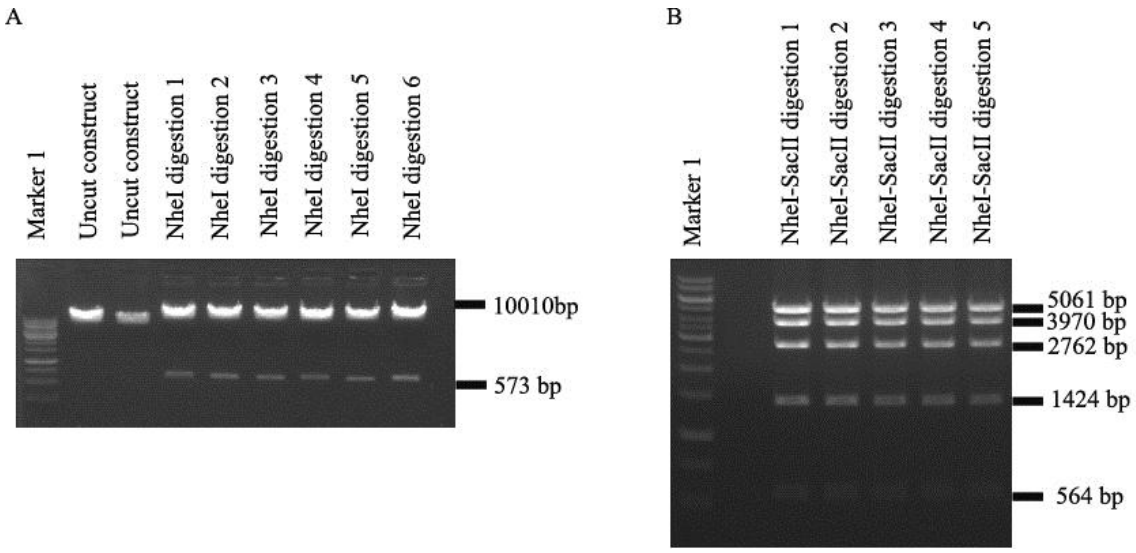

Figure 5.22. Restriction digestion of pP{white-STAR} containing the 3' homology arm (A) and both 3' and 5' homology arm (B).

After generating the targeting vector containing the up- and down-stream homology arms of *mtm*, its bacterial clone was sent to Genetic Services, Inc., USA, for site directed injection. Flies having a landing site, *attP2*, on their third chromosome were selected and the vector was injected into embryos of these flies.

5.3.2. Homologous Recombination using IMAGO

After obtaining the fly lines which carry the targeting vector for mtm in their genome, the landing site of the insertion was mapped. Male flies obtained from injections were crossed with *yw* virgin flies. All of the males among their progeny had white eyes, indicating that the insertion was on the X-chromosome.

In order to mobilize the vector, male flies carrying the insertion, were crosses with female virgin flies of *hs:Flp,hs:ISce-I/TM3, hs:hid* genotype. The larvae were given one hour heat shock at 38ºC for 2 days, so that Flippase and ISce-I enzymes were expressed. It was expected that the vector would flip out from the insertion site by Flippase and be linearized by the ISce-I activity. So, homologous recombination would occur in some of the cells that would be detected in the in the progeny flies with mosaic eye color would be obtained (Figure 5.23). For targeting *mtm*, 100 crossses were set, however, all of the flies

in their progeny had red eyes. If homologous recombination occurs in germ line cells, fly with red eye will come out after crossing the mosaic flies with yw.

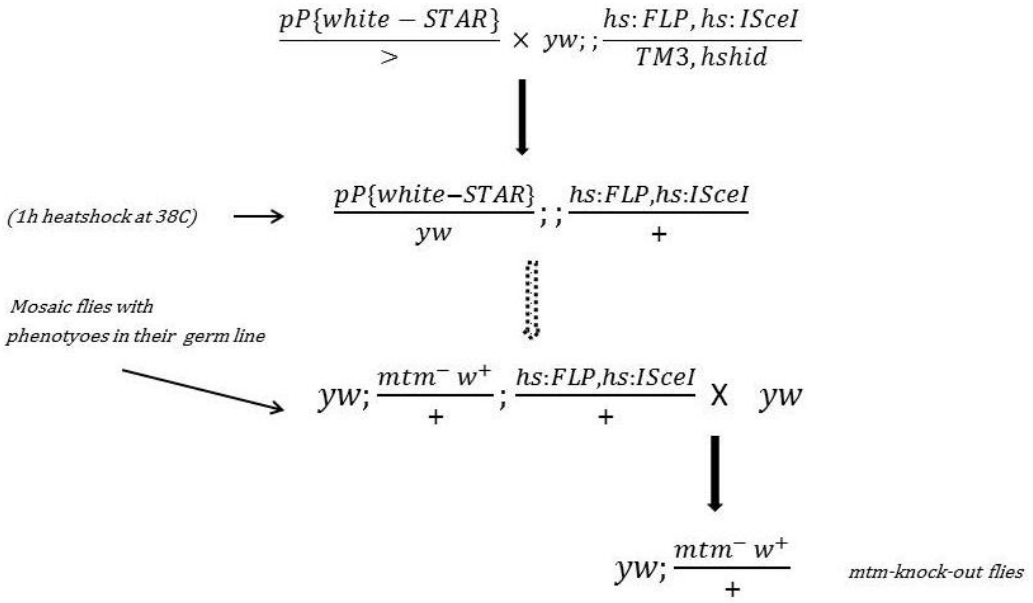

Figure 5.23. Targeting mtm *via* homologous recombination. Flies carrying the targeting vector *pP{white-STAR}* were crossed with *hs:Flp, hs:ISce-I* flies.

6. DISCUSSION

Mutations in *MTMR2* are associated with the demyelinating recessive CMT (CMT4B1), and a loss of function effect on the disease phenotype. In this study, we firstly tried to identify the role of mtm which is the fly homolog of MTMR2 by analyzing the neuromuscular junctions (NMJs) of flies. The deletion of *mtm* showed disrupted shape of the boutons which are the connections between motor nerve terminals with muscles. In immunohistochemistry experiments, it was observed that the mutants showed excess small boutons, called satellite boutons. The functional analysis by using FM 1-43 dye uptake assay showed the presence of satellite boutons and subboutonic structures in the NMJs. The ubiquitous and neuronal down-regulation of mtm using RNAi also resulted in satellite bouton structure, indicating that both partial deletion of mtm and its down-regulation by RNAi have similar phenotypes. In the second part of the study, we tried to generate a CMT4B1 model in flies using integrase-mediated approach for gene knock out (IMAGO) in order to delete *mtm* precisely and replace it with human MTMR2, as well as mutant versions of MTMR2. The targeting vector was successfully generated; however, deletion of *mtm* did not take place in the initial screenings performed so far.

The aim of the study is to understand CMT4B1 pathogenesis and the function MTMR2 protein. The previous studies indicate that MTMR2 is an important phospholipid phosphatase. In cell culture experiments, it was shown that MTMR2 dephosphorylates PI3P and PI(3,5)P_2 and has a role in endosomal trafficking (Cao *et al*., 2008; Tsujita *et al*., 2004). It is thought that the lack of MTMR2 activity causes impaired PI metabolism and accumulation of PI3P and PI(3,5)P_2 vesicle pools, affecting membrane trafficking. In CMT4B1, excess membrane formation in Schwann cells accounts for myelin outfoldings.

Although mutations in MTMR2 cause a demyelination phenotype, it was observed that it interacts with PSD-95 protein, which is a post-synaptic protein predominantly found in excitatory synapses (Lee *et al*., 2010). This study showed that MTMR2 might also have a functional role not only in Schwann cells, but also in neurons. In a *Mtmr2* null mouse model, it was observed that Mtmr2 functionally interacts with Fig4 in both neurons and Schwann cells, having opposite effects in the regulation of PI(3,5)P_2 (Vaccari *et al.*, 2011).

As MTMR2 regulates PI lipids and it functionally interacts with neuronal proteins, it can be speculated that MTMR2 has a function in PI-metabolism in neurons. However, the functional role of MTMR2 in neurons has not been assessed. In order to study the function of MTMR2 in neurons, we chose *Drosophila* as a model organism, because proteins regulating the PI metabolism are well conserved between *Drosophila* and human (Slabbaert *et al*., 2012).

NMJs are the areas where neurons interact with muscles. They have been used to understand the mechanisms mechanisms of synaptic proteins trafficking, because synapses are zones with frequent vesicular trafficking in which neurotransmitters are released and taken up continuously by endo- and exocytosis. The proteins involved in PI metabolism have also been studied extensively in the NMJ (Slabbert *et al.*, 2012). Thus, the larval *Drosophila* NMJ provides a good opportunity to understand the synaptic vesicular trafficking, as the NMJs of the third instar larva are easily accessible and various sophisticated assays have been generated to analyze the NMJ structure and function.

As most of the proteins in the PI-metabolism are conserved between *Drosophila* and human, mtm, the *Drosophila* homolog of human MTMR2, was chosen for investigation of its mechanisms of action related to CMT phenotypes. It has been shown previously that mtm has a role in regulation of endosomal PI3P pools and cortical remodeling in immune cells (Velichkova *et al*., 2010). But, its neuronal function remains unclear.

In the first part of this study, the role of mtm in neurons was investigated by studying the larval NMJ. For this purpose, loss of function mutants of mtm ($mtm^{\Delta 77,}$ $mtm^{\Delta 210}$ and $mtm^{\Delta 77/z2\text{-}4747}$) and and *mtm* RNAi line were used and effects on the NMJ morphology and function were analyzed. In the second part, a strategy to develop a *Drosophila* model CMT4B1 was constructed.

6.1. NMJ Analysis of *mtm* Mutants

The *mtm* null mutant flies ($mtm^{\Delta 77}$, $mtm^{\Delta 210}$ and $mtm^{\Delta 77/z2\text{-}4747}$) exhibited lethality at the third instar larval stage indicating that it is important for the development of the fly

(Velichkova *et al.*, 2010). In order to analyze how effects of *mtm* mutations can be related to CMT disease phenotypes, the NMJ morphology was studied in third instar larva.

6.1.1. Morphological Analysis via Immunohistochemistry

In immunohistochemistry experiments, the compound heterozygous larva carrying two different null alleles showed abnormal NMJ structure with an excess number of boutons of smaller size, called satellite boutons. Four different antibodies against synaptic proteins were used in order to determine the NMJ morphology; DLG is a post-synaptic protein and it labels areas of muscle-neuron interaction; HRP is an oxidase found on the neuronal membrane; CSP is localized to presynaptic boutons and synapsin is found on the neurotransmitter vesicles in presynapses. All of the *mtm* null mutants showed that the NMJ morphology is different from the wild type in DLG and HRP stainings. This staining revealed primarily post-synaptic morphology differences and the presence of satellite boutons. In order to visualize the presynaptic morphology, CSP and synapsin stainings were performed along with HRP in $mtm^{\Delta 77}/mtm^{\Delta 210}$ larvae. The observation of satellite boutons in this mutant background indicates that neurons also contribute to distortion of the NMJ morpholog. In addition to the appearance of satellite boutons, the shape of boutons was irregular compared to that of normal NMJs. Thus, the loss of mtm leads to impaired NMJ and appearance of satellite boutons.

In NMJ analyses of *Drosophila* models for some neurodegenerative diseases, like spastic hereditary paraplegia, multiple sclerosis or Huntington's disease, satellite boutons with smaller NMJ size have beeb observed (*Bayat et al*., 2011). Thus, the NMJ size is an important indicator of NMJ growth. In these disease models, it was speculated that disease-related proteins have a role in NMJ growth by interacting with cytoskeletal proteins. The impaired functioning of these proteins results in smaller NMJs. In order to understand whether *mtm* mutations change the NMJ size, the length of the NMJs were measured and their ratio to the innervated muscle area was calculated. Only the NMJs innervating muscle 6-7 in the A2 segment were chosen for this quantification, because the size and shape of each NMJ on different muscles changes. The NMJ on muscle 6-7 in the A2 segment is a good candidate to perform statistical analysis, as it is one of the largest NMJ in the larvae, and has a distinct shape, that makes it easy to differentiate from other NMJs. The statistical

analysis was done with control and $mtm^{\Delta 77}/mtm^{\Delta 210}$ larvae and showed that the NMJ/muscle ratio of the mutants was not significantly different from the control (two-tailed p-value=0.3775). From these data, we speculate that the NMJ morphology differences in mutants are not by disrupted interactions of mtm with cytoskeletal proteins in neurons. However, these data should be strengthened by testing the morphology of cytoskeletal proteins in the NMJ as well.

RNAi lines were used to down-regulate *mtm*'s expression spatiotemporally, in order to observe the loss of function effect easily. An RNAi line from TRIP library was used, and this line was crossed with different driver lines to study effect of down-regulation organism-wide and in neurons. Use of RNAi has not only been effective and time saving, but also vital as we did not have precise deletion alleles. The *mtm* null mutants generated by Velichkova and co-workers were *P*-element excision alleles and resulted in the delition of an additional gene upstream of *mtm* with unknown function, *CG9117*. In order to investigate whether the observed null phenotypes were caused only by lack of *mtm* and in order to allow for spatial and temporal down-regulation of *mtm*, the *mtm* gene was down-regulated by RNAi. The *mtm* RNAi was expressed using various drivers including ubiquitous, motor neuron-specific and presynaptic drivers. The ubiquitous down-regulation of *mtm* using an actin5C-driver resulted in pupal lethality; no adult flies were observed. From this, it can be concluded that mtm has an essential function for the survival of the flies.

The NMJ morphology was analyzed in third instar larva by pre- and postsynaptic antibodies for each driver line. When *mtm* was down-regulated ubiquitously using actin5C driver, satellite boutons were observed in DLG-HRP and CSP-HRP stainings. Although the NMJs did not show an excess amount of satellite boutons, the ubiquitous down-regulation of *mtm* shows a similar although not exactly the same effect, to the phenotype observed in null mutants. This difference in severe might be due to the incomplete silencing of *mtm* by RNAi. It also needs to be established if the downregulation of *CG9117* has an effect on NMJ structure to exclude that the severe phenotype observed in the mutants results from the additive effect of lack of both genes. Additionally, the effect of the RNAi can be increased by adding a copy of UAS-Dicer, which has been shown to

increase RNAi effects in neurons or increasing the copy numbers of the driver and RNAi alleles (Vermeulen *et al.*, 2005).

The down-regulation of *mtm* via RNAi in motor neurons and presynapses using OK6 and n-Syb-Gal4 drivers, respectively, also resulted in satellite boutons in the NMJs of the larva similar to the results obtained by its ubiquitous down-regulation. Thus, silencing of *mtm* function specifically in neurons is sufficient to generate a phenotype comparable to the phenotypes observed in null mutants. This suggests that mtm functions in motor neurons and contributes to abnormal satellite bouton morphology in the NMJ of third instar larvae.

6.1.2. Functional Analysis via FM 1-43 Dye Uptake Assay

FM 1-43 is a lipophilic dye and non-fluorescent in aqueous medium. It fluoresces when bound to lipid membranes. Alive larvae stimulated either chemically or electrically take up FM 1-43 by endocytosis and the bound dye starts to fluoresce. Thus the morphology and the functioning of the NMJ boutons can be analyzed by measuring the level of fluorescence intensity. The FM 1-43 dye uptake assay is solely based on endo- and exocytosis events; therefore, it helps to gain insights into membrane trafficking mechanisms in the NMJ. This assay has critical importance in understanding the mechanism of action of mtm in the synapses.

FM 1-43 dye uptake assay was performed in order to evaluate the structural and functional differences between $mtm^{\Delta 77}$/ $mtm^{\Delta 210}$, $mtm^{\Delta 77}$/ $mtm^{\Delta 77/z2\text{-}4747}$ and control larvae. While *mtm* null mutants showed a distorted NMJ structure with satellite boutons as observed in immunohistochemistry experiments, control larvae exhibited spherical and smooth boutons in their NMJs. An interesting observation was that the mutants had submembrane inclusions which were seen as subboutonic structures. As FM 1-43 fluoresces only when bound to endosomes, it can be said that there were endosomes which either took up the dye in gross amounts or vesicles were fused together forming subboutonic inclusions that resulted in dye accumulation.

Considering the first fate, the level of fluorescence intensity was measured for the mutants and the controls, and statistical analysis was performed. Since no significant difference was observed in the overall fluorescence intensity, it can be assumed that the overall dye uptake was not increased in mutants. Therefore, the only explanation for high fluorescence in submembrane inclusions is that these vesicles cannot participate in the endosomal trafficking as they should. It is most probable that the vesicles fluorescing with high intensity are early and late endosomes, where PI3P, the target of mtm is localized. If the phosphatase activity of mtm is absent, vesicles harboring PI3P would be observed in early and late endosomes (Figure 6.1). Future experiments should include characterization of the PI pools in synapses and investigatigaiton of whether these PI pools and the submembrane inclusions co-localize. In this way, it could be concluded whether PI lipids which are targets of mtm are effectors in the perturbation of this mechanism (Figure 6.2).

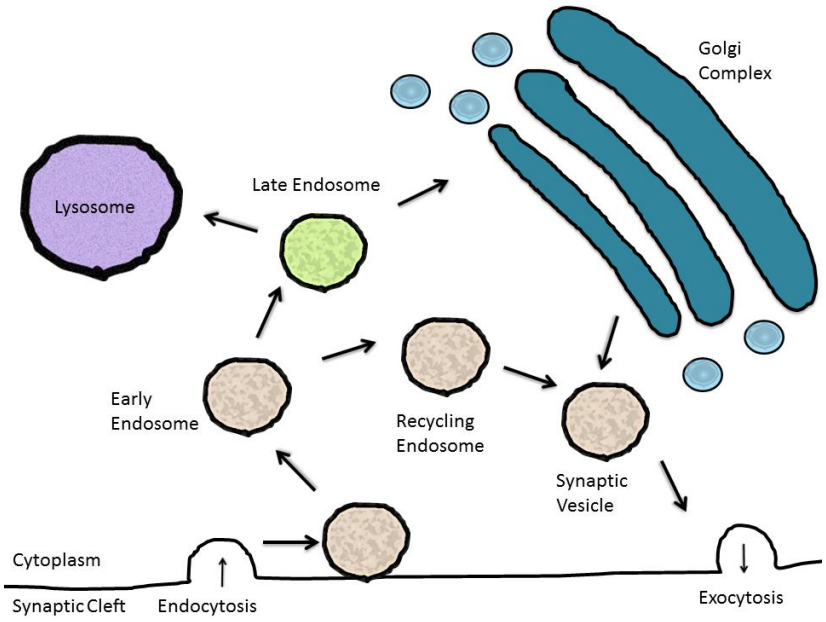

Figure 6.1. Vesicular trafficking in the presynaptic zone.

6.2. Targeting mtm *via* Homologous Recombination

P-element excision mutants and RNAi lines of *mtm* provide an understanding of how mtm contributes to synaptic morphology and function in the NMJ of *Drosophila* larvae. However, in order to study MTMR2 function and reveal its roles in neurons, and how its mutations cause the disease phenotype, a precise deletion of *mtm* and its replacement with

wild type and mutant human *MTMR2* are necessary. Homologous recombination provides a useful tool to target *mtm* and knock-in any gene of interest in place of the coding region of the gene leaving regulatory elements in the 5’ and 3’ regions intact.

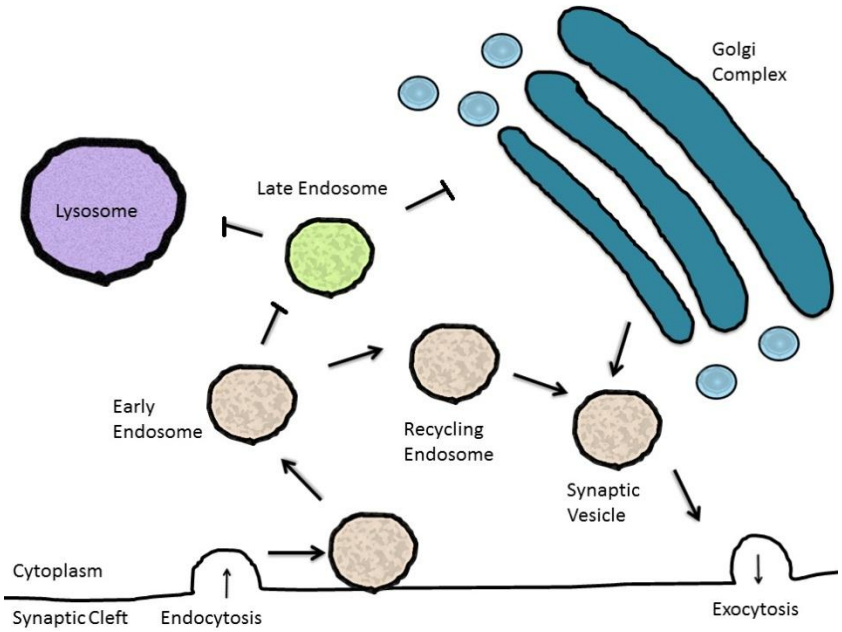

Figure 6.2. Lack of mtm might affect the vesicular trafficking in the presynaptic zone.

Instead of classical ends-out homologous recombination, an integrase-mediated approach for gene knock-out (IMAGO) was used in the study. The *mtm*-targeting vector was generated by cloning the 5’ and 3’ regions flanking the coding region of *mtm* into the pP{white-STAR} vector backbone. This construct was injected into flies, harboring *attP*2 landing sites on their third chromosome. Chromosome mapping showed that the insert was localized to the X chromosome, instead of the third. The initial crosses to mobilize and recombine the marker gene with *mtm*, were performed. However, none of the progeny screened had *mtm* deletions. Therefore, the screening for mutants should continue in order to generate *mtm*-deficient fly lines.

mtm is located on the left arm of the second chromosome. The integration site of the targeting vector was desired not to be found in the same chromosome with *mtm*, because the integration and the mobilization of the vector may change the DNA sequence, where it is integrated, and result in an unwanted genotype. Choosing a different chromosome for integration is more feasible, as it is possible to get rid of the integration chromosome by

crossing it with wild type or balancer lines. The reason for not choosing the integration chromosome as the second is that we want to obtain flies that differ from wild type only mtm gene with no other mutations in different parts of the genome.

As *Drosophila* has four chromosome pairs, we could choose one of the other 3 chromosomes. The fourth chromosome is a tiny chromosome and there is not any balancer chromosome for the fourth one. It is more likely that the integration occurs in other chromosomes, the X and the third chromosomes were the two options that we had. However, we have chosen the third chromosome, because the balancer chromosomes for the X chromosome do not provide homozygous lethality and it is hard to track the homozygous lines for the integrated vector. Therefore, the third chromosome was selected and site-directed integration was performed using flies with attachment sites, attP2, on their third chromosome. It was expected that our targeting vector would integrase into that site. However, the integration is overall a random process; even the attachment sites increase the likelihood that the vector integrates on that attachment site, it is still possible that the integration occurs into any other chromosomes. In this study, the targeting vector was integrated into the X-chromosome after injection. Although it was not desired as landing chromosome, it does not affect the homologous recombination process, because the second chromosome where *mtm* resides was intact with no insertion.

It was tried to mobilize the vector by expressing heat shock sensitive flippase and ISce-I enzymes and expected that homologous recombination occurred between the linearized vector and the flanking regions of mtm. This process could be tracked by the eye color marker. As the vector was injected to flies with white eye color, the flies carrying the vector had red eye marker. These flies were crossed with *hs:Flp, hs:ISce-I* flies and their progeny were given heat-shock to express that enzymes in the second instar larval stage. It was expected that adult flies would have mosaic eyes with red and white patches, showing that the vector was flipped out from the genome (white eye) and recombined with *mtm* (red eye). Out of 100 crosses, no mosaic eye was observed and all of the flies had red eyes with no patches, suggesting that vector were not mobilized. This might be because the flippase was not expressed or was not efficient to carry out the mobilization of the vector. On the other hand, homologous recombination is a very difficult technique; it is affected by

various factors, such as; the duration of heat shock and the genomic region of the gene of interest. Thus, it has to be set and screened more crosses.

The reason for choosing IMAGO instead of classical homologous recombination is, because it is possible to use recombinase-mediated cassette exchange (RMCE) to easily knock-in any target sequence between *attP* attachment sites. Our future experiments include knocking-in the following coding sequences including wild type *MTMR2*, mutant forms of *MTMR2*, *Gal4* and *mCherry*. Using *MTMR2* expressing flies, it will be possible to test whether *MTMR2* rescues *mtm*-deficiency, and thus conclude whether mtm and MTMR2 are functional homologs. Flies expressing mutant forms of *MTMR2* will be analyzed in terms of CMT-like phenotypes, in terms of cellular morphology (immunohistochemistry and electron microscopy), function (FM 1-43 dye uptake assays and electrophysiology), behavior (larval crawling, negative geotaxis and sensory assays) and finally longevity assays. Besides replacement of *mtm* using wild type and mutant *MTMR2*, the *mtm* gene is planned to be overexpressed spatially and temporally in *mtm* deficient flies in order to determine the developmental stage at which *mtm* function is necessary.

7. CONCLUSION

In this study, we focused on generating a CMT4B1 *Drosophila* model and have established the methodology to analyze the lines that we planned to generate. We have used NMJ immunohistochemistry and FM 1-43 dye uptake assays as methodologies to analyze available mutants and RNAi lines. The future study comprises the generation of wild type and mutant *MTMR2* knock-in lines, and analysis of these flies and to establish if they recapitulate the symptoms of the peripheral neuropathy, CMT. Thereby, we will be able to generate CMT4B1 disease model to understand MTMR2 function and CMT pathogenesis. Thus, in the future it will be possible to perform chemical screens to identify potential therapeutic agents that target CMT4B1 pathogenesis.

REFERENCES

Adams, M.D., S.E. Celniker, R.A. Holt, C.A. Evans, J.D. Gocayne, P.G. Amanatides, S.E. Scherer, P.W. Li, R.A. Hoskins, R.F. Galle *et al.*, 2000, "The Genome Sequence of *Drosophila melanogaster*", *Science*, Vol. 287, No. 5461, pp. 2185-2195.

Adams, M.D. and J.J Sekelsky, 2002, "From Sequence to Phenotype: Reverse Genetics in *Drosophila melanogaster*", *Nature Reviews Genetics*, Vol. 3, No. 3, pp. 189-198.

Altschul, S.F., T.L. Madden, A.A. Schäffer, J. Zhang, Z. Zhang, W. Miller, and D.J. Lipman, 1997, "Gapped BLAST and PSI-BLAST: a New Generation of Protein Database Search Programs", *Nucleic Acids Research*, Vol. 25, No. 17, pp. 3389-3402.

Azzedine H., A. Bolino, T. Taïeb, N. Birouk, M. Di Duca, A. Bouhouche, S. Benamou, A. Mrabet, T. Hammadouche, T. Chkili *et al.*, 2003, "Mutations in MTMR13, a New Pseudophosphatase Homologue of MTMR2 and Sbf1, in Two Families with an Autosomal Recessive Demyelinating Form of Charcot-Marie-Tooth Disease Associated with Early-Onset Glaucoma", *American Journal of Human Genetics*, Vol. 72, No. 5, pp. 1141-1153.

Barisic, N., K.G. Claeys, M. Sirotković-Skerlev, A. Löfgren, E. Nelis, P. De Jonghe, and V. Timmerman, 2008, "Charcot-Marie-Tooth Disease: a Clinico-Genetic Confrontation", *Annals of Human Genetics*, Vol. 72, No. 3, pp. 416-441.

Bayat, V., M. Jaiswal, and H.J. Bellen, 2011, "The BMP Signaling Pathway at the *Drosophila* Neuromuscular Junction and its Links to Neurodegenerative Diseases", *Current Opinion in Neurobiology*, Vol. 21. No.1, pp. 182-188.

Begley, M.J., G.S. Taylor, M.A. Brock, P. Ghosh, V.L. Woods, and J.E. Dixon, 2006, "Molecular Basis for Substrate Recognition by MTMR2, a Myotubularin Family

Phosphoinositide Phosphatase", *Proceedings of the National Academy of Sciences of the United States of America,* Vol. 103, No. 4, pp. 927-932.

Bellen, H.J., V. Budnik W, R.S. Hawley RS, M. Ashburner, and B. Sullivan, 2000, *Drosophila Protocols*, Cold Spring Harbor Laboratory Press, New York.

Berger, P., S. Bonneick, S. Willi, M. Wymann, and U. Suter, 2002, "Loss of Phosphatase Activity in Myotubularin-Related protein 2 is Associated with Charcot-Marie-Tooth Disease Type 4B1", *Human Molecular Genetics,* Vol. 11, No. 13, pp. 1569-1579.

Berger, P., C. Schaffitzel, I. Berger, N. Ban, and U. Suter, 2003, "Membrane Association of Myotubularin-Related Protein 2 is Mediated by a Pleckstrin Homology-GRAM Domain and a Coiled-Coil Dimerization Module", *Proceedings of the National Academy of Sciences of the United States of America,* Vol. 100, No. 21, pp. 12177-12182.

Betz, W.J. and G.S. Bewick, 1992, "Optical Analysis of Synaptic Vesicle Recycling at the Frog Neuromuscular Junction", *Science,* Vol. 255, No. 5041, pp. 200-203.

Bi, X. and Y.S. Rong, 2003, "Gene Manipulation by Homologous Recombination in *Drosophila*", *Briefings in Functional Genomics and Proteomics,* Vol. 2, No. 2, pp. 142-146.

Bilder, D., 2001, "PDZ Proteins and Polarity: Functions from the Fly", *Trends in Genetics*, Vol. 17, No. 9, pp. 511-519.

Bolino, A., M. Muglia, F.L. Conforti, E. LeGuern, M.A. Salih, D.M. Georgiou, K. Christodoulou, I. Hausmanowa-Petrusewicz, P. Mandich, A. Schenone *et al.,* 2000, "Charcot-Marie-Tooth Type 4B is Caused by Mutations in the Gene Encoding Myotubularin-Related Protein-2", *Nature Genetics*, Vol. 25, No. 1, pp. 17-19.

Bolino, A., A. Bolis, S.C. Previtali, G. Dina, S. Bussini, G. Dati, S. Amadio, U. Del Carro, D.D. Mruk, M.L. Feltri, C.Y. Cheng, A. Quattrini, and L. Wrabetz, 2004,

"Disruption of Mtmr2 Produces CMT4B1-like Neuropathy with Myelin Outfolding and Impaired Spermatogenesis", *The Journal of Cell Biology*, Vol. 167, No. 4, pp. 711-721.

Bolis, A., S. Coviello, I. Visigalli, C. Taveggia, A. Bachi, A.H. Chishti, T. Hanada, A. Quattrini, S.C. Previtali, A. Biffi *et al.*, 2009, "Dlg1, Sec8, and Mtmr2 Regulate Membrane Homeostasis in Schwann Cell Myelination", *The Journal of Neuroscience*, Vol. 29, No. 27, pp. 8858-8870.

Bonini, N.M. and A.D. Gitler, 2011, "Model Organisms Reveal Insight into Human Neurodegenerative Disease: Ataxin-2 Intermediate-Length Polyglutamine Expansions are a Risk Factor for ALS", *Journal of Molecular Neuroscience*, Vol. 45, No. 3, pp. 676-683.

Brand, A.H. and N. Perrimon, 1993, "Targeted Gene Expression as a Means of Altering Cell Frates and Generating Dominant Phenotypes", *Development*, Vol. 118, No. 2, pp. 401-415.

Bullock, T.H., D.S. Faber, and H. Korn, 1978, *Neurobiology of the Mauthner Cell"*, Raven Press, New York.

Cao, C., J.M. Backer, J. Laporte, E.J. Bedrick, and A. Wandinger-Ness, 2008, "Sequential Actions of Myotubularin Lipid Phosphatases Regulate Endosomal PI(3)P and Growth Factor Receptor Trafficking", *Molecular Biology of the Cell*, Vol. 19, No. 8, pp. 3334-3346.

Chance, P.F., M.K. Alderson, K.A. Leppig, M.W. Lensch, N. Matsunami, B. Smith, P.D. Swanson, S.J. Odelberg, C.M. Disteche, and T.D. Bird, 1993, "DNA Deletion Associated with Hereditary Neuropathy with Liability to Pressure Palsies", *Cell*, Vol. 72, No. 1, pp. 143-151.

Choi, C.M., S. Vilain, M. Langen, S. Van Kelst, N. De Geest, J. Yan, P. Verstreken, and B.A. Hassan, 2009, "Conditional Mutagenesis in *Drosophila*", *Science,* Vol. 324, No. 5923, p. 54.

Denu, J. and J.E Dixon, 1998, "Protein Tyrosine Phosphatases: Mechanisms of Catalysis and Regulation", *Current Opinion in Chemical Biology*, Vol. 2, No. 5, pp. 663-641.

Dietzl, G., D. Chen, F. Schnorrer, K.C. Su, Y. Barinova, M. Fellner, B. Gasser, K. Kinsey, S. Oppel, S. Scheiblauer *et al.*, 2007, "A Genome-wide Transgenic RNAi Library for Conditional Gene Inacitivation in *Drosophila*", *Nature*, Vol. 447, No. 7150, pp. 151-156.

Di Paolo, G. and P. De Camilli, 2006, "Phosphoinositides in Cell Regulation and Membrane Dynamics", *Nature*, Vol. 443, No. 7112, pp. 651-657.

Doerks, T., M. Strauss, M. Brendel, and P. Bork, 2000, "GRAM, a Novel Domain in Glycosyltransfereases, Myotubularins and Other Putative Membrane-Associated Proteins", *Trends in Biochemical Sciences,* Vol. 25, No. 10, pp. 483-485.

Dubourg, O., H. Azzedine, C. Verny, G. Durosier, N. Birouk, R. Gouider, M. Salih, A. Bouhouche, A. Thiam, D. Grid *et al.*, 2006, "Autosomal-Recessive Forms of Demyelinating Charcot-Marie-Tooth Disease", *Neuromolecular Medicine,* Vol. 8, No. 1-2, pp. 75-86.

Duffy, J.B., 2002, "Gal4 System in Drosophila: a Fly Geneticist's Swiss Army Knife", *Genesis*, Vol. 34, No. 1-2, pp. 1-15.

Dyck, P. J., P. Chance, R. Lebo, J.A. Carney and P.K. Thomas, 1993, *Peripheral Neuropathy*, 3rd edition, W.B. Saunders, Philadelphia.

Fischer, J.A., E. Giniger, T. Maniatis, and M. Ptashne, 1988, "Gal4 Activates Transcription in *Drosophila*", *Nature*, Vol. 332, No. 6167, pp. 853-856.

Giniger, E., S.M. Varnum, and M. Ptashne, 1985, "Specific DNA Binding of Gal4, a Positive Regulatory Protein of Yeast", *Cell*, Vol. 40, No. 4, pp. 767-774.

Greenspan, R. J., 2004, *Fly Pushing: The Theory and Practice of Drosophila Genetics*, 2nd edition, Cold Spring Harbor Laboratory Press, New York.

Guan, K.L. and J.E. Dixon, 1991, "Evidence for Protein-Tyrosine-Phosphatase Catalysis Proceeding *via* a Cysteine-Phosphate Intermediate", *The Journal of Biological Chemistry*, Vol. 266, No. 26, pp. 17026-17030.

Harding, A.E. and P.K. Thomas, 1980, "Clinical Aspects of Heridatry Motor and Sensory Neuropathy Types I and II", *Brain*, Vol. 103, No. 2, pp. 259-280.

Houlden, H., R.H. King, N.W. Wood, P.K. Thomas, and M.M. Reilly, 2001, "Mutations in the 50 Region of the Myotubularin-Related Protein 2 (MTMR2) Gene in Autosomal Recessive Hereditary Neuropathy with Focally Folded Myelin", *Brain*, Vol. 124, No. 5, pp. 907-915.

Imlach, W. and B.D. McCabe, 2009, "Electrophysiological Methods for Recording Synaptic Potentials from the NMJ of *Drosophila* Larvae", *Journal of Visualized Experiments*, Vol. 6, No. 24, p. 1109.

Jordanova, A., J. Irobi, F.P. Thomas, P. Van Dijck, K. Meerschaert, M. Dewil, I. Dierick, A. Jacobs, E. De Vriendt, V. Guergueltcheva *et al.*, 2006, "Disrupted Function and Axonal Distribution of Mutant Tyrosyl-Trna Synthetase in Dominant Intermediate Charcot-Marie-Tooth Neuropathy", *Nature Genetics*, Vol. 38, No. 2, pp. 197-202.

Kerk, D. and G.B. Moorhead, 2010, "A Phylogenetic Survey of Myotubularin Genes of Eukaryotes: Distribution, Protein Structure, Evolution, and Gene Expression", *BMC Evolutionary Biology*, Vol. 10, No. 196, pp. 1-16.

Kim, S.A., P.O. Vacratsis, R. Firestein, M.L. Clearly, and J.E. Dixon, 2003, "Regulation of Myotubularin-Related (MTMR)2 Phosphatidylinositol Phosphatase by MTMR5, a

Catalytically Inactive Phosphatase", *Proceedings of the National Academy of Sciences of the United States of America*, Vol. 100, No. 8, pp. 4492-4497.

Krauss, M. and V. Haucke, 2007, "Phosphoinositides: Regulators of Membrane Traffic and Protein Function", *FEBS Letters*, Vol. 581, No. 11, pp. 2105-2111.

Laporte, J., L.J. Hu, C. Kretz, J.L. Mandel, P. Kioschis, J.F. Coy, S.M. Klauck, A. Poustka, and N. Dahl, 1996, "A Gene Mutated in X-Linked Myotubular Myopathy Defines a New Putative Tyrosine Phosphatase Family Conserved in Yeast", *Nature Genetics*, Vol. 13, No. 2, pp. 175-182.

Lee H.W., Y. Kim, K. Han, H. Kim, and E. Kim, 2010, "The Phosphoinositide 3-Phosphate MTMR2 Interacts with PSD-95 and Maintains Excitatory Synapsis by Modulating Endosomal Traffic", *The Journal of Neuroscience*, Vol. 30, No. 26, pp. 5508-5518.

Lupski, J.R., R.M. De Oca-Luna, S. Slaugenhaupt, L. Pentao, V. Guzzetta, B.J. Trask, O. Saucedo-Cardenas, D. F. Barker, J.M. Killian, C.A. Garcia *et al.*, 1991, "DNA Duplication Associated with Charcot-Marie-Tooth Disease Type 1A", *Cell*, Vol. 66, No. 2, pp. 219-232.

Meinertzhagen, I.A., 2010, "The Organization of Invertebrate Brains: Cells, Synapses and Circuits", *Acta Zoologica*, Vol. 91, No. 1, pp. 64–71.

Moloney, A., D.B. Sattelle, D.A. Lomas, and D.C. Crowther, 2010, "Alzheimer's Disease: Insights from *Drosophila melanogaster* Models", *Trends in Biochemical Sciences*, Vol. 35, No. 4, pp. 228-235.

Murphy, S.M., M. Laura, K. Fawcett, A. Pandraud, Y.T. Liu, G.L. Davidson, A.M. Rossor, J.M. Polke, V. Castleman, H. Manji *et al.*, 2012, "Charcot-Marie-Tooth Disease: Frequency of Genetic Subtypes and Guidelines for Genetic Testing", *Journal of Neurology, Neurosurgery and Psychiatry*, Vol. 83, No. 7, pp. 706-710.

Nakhro, K., J.M. Park, Y.B. Hong, J.H. Park, S.H. Nam, B.R. Yoon, J.H. Yoo, H. Koo, S.C. Jung, H.L. Ki *et al.*, 2013, "SET Binding Factor 1 (SBF1) Mutation Causes Charcot-Marie-Tooth Disease Type 4B3", *Neurology*, Vol. 81, No. 2, pp. 165-173.

Nelis, E., S. Erdem, E. Tan, A. Löfgren, C. Ceuterick, P. De Jonghe, C. Van Broeckhoven, V. Timmerman, and H. Topaloglu, 2002, "A Novel Homozygous Missense Mutation in the Myotubularin-Related Protein 2 Gene Associated with Recessive Charcot-Marie-Tooth Disease with Irregularly Folded Myelin Sheaths", *Neuromuscular Disorders*, Vol. 12, No. 9, pp. 869-873.

Pareyson, D. and C. Marchesi, 2009, "Diagnosis, Natural History, and Management of Charcot–Marie–Tooth Disease", *Lancet*, Vol. 8, No. 7, pp. 654-667.

Parman, Y., E. Battaloglu, I. Baris, B. Bilir, M. Poyraz, N. Bissar-Tadmouri, A. Williams, N. Ammar, E. Nelis, V. Timmerman *et al.*, 2004, "Clinicopathological and Genetic Study of Early-Onset Demyelinating Neuropathy", *Brain*, Vol. 125, No. 11, pp. 2540-2550.

Previtali S.C., B. Zerega, D.L. Sherman, P.J. Brophy PJ, G. Dina, R.H. King, M.M. Salih, L. Feltri, A. Quattrini, R. Ravazzolo *et al.*, 2003, "Myotubularin-Related 2 Protein Phosphatase and Neurofilament Light Chain Protein, both Mutated in CMT Neuropathies, Interact in Peripheral Nerve", *Human Molecular Genetics*, Vol. 12, No. 14, pp. 1713-1723.

Quattrone, A., A. Gambardella, F. Bono, U. Aguglia, A. Bolino, A.C. Bruni, M.P. Montesi, R.L. Oliveri, M. Sabatelli, O. Tamburrini *et al.*, 1996, "Autosomal Hereditary Motor and Sensory Neuropathy with Focally Folded Myelin Sheaths: Clinical, Electrophysiologic and Genetic Aspects of a Large Family", *Neurology*, Vol. 46, No. 5, pp. 1318-1324.

Robinson, F.L. and J.E. Dixon, 2005, "The Phosphoinositide-3-phosphatase MTMR2 Associates with MTMR13, a Membrane-Associated Pseudophosphatase also

Mutated in Type 4B Charcot-Marie-Tooth Disease", *The Journal of Biological Chemistry*, Vol. 280, No. 36, pp. 31699-31707.

Rong, Y.S. and K.G. Golic, "Gene Targeting by Homologous Recombination in *Drosophila*", *Science*, Vol. 288, No. 5473, pp. 2013-2018.

Schuster, C.M., G.W. Davis, R.D. Fetter, and C.S. Goodman, 1996, "Genetic Dissection of Structural and Functional Components of Synaptic Plasticity. I. Fasciclin II Controls Synaptic Stabilization and Growth", Neuron, Vol. 17, No. 4, pp. 641-654.

Skre, H., 1974, "Genetic and Clinical Aspects of Charcot-Marie-Tooth's Disease", *Clinical Genetics*, Vol. 6, No. 2, pp. 98-118.

Slabbaert, J.R., T.M. Khuong, and P. Verstreken, 2012, "Phosphoinositides at the Neuromuscular Junction of *Drosophila melanogaster*: a Genetic Approach", *Methods in Cell Biology*, Vol. 108, No. 1, pp. 227-247.

Suter, U. and S.S. Scherer, 2003, "Disease Mechanisms in Inherited Neuropathies", *Nature Reviews Neuroscience*, Vol. 4, No. 9, pp. 714-726.

Tazir, M., M. Bellatache, S. Nouioua, and J.M. Vallat, 2013, "Autosomal Recessive Charcot-Marie-Tooth Disease: from Genes to Phenotypes", *Journal of the Peripheral Nervous System*, Vol. 18, No. 1, pp. 113-129.

Tosch, V., H.M. Rohde, H. Tronchère, E. Zanoteli, N. Monroy, C. Kretz, N. Dondaine, B. Payrastre, J.L. Mandela, and J. Laporte, 2006, "A novel PtdIns3P and PtdIns(3,5)P2 Phosphatase with an Inactivating Variant in Centronuclear Myopathy", *Human Molecular Genetics*, Vol. 15, No. 21, pp. 3098-3106.

Tsujita, K. T. Itoh, T. Ijuin, A. Yamamoto, A. Shisheva, J. Laporte, and T. Takenava, 2004, "Myotubularin Regulates The Function of the Late Endomose Through the Gram-Domain-Phophatidylinositol 3,5—Bisphosphate Interaction", *Journal of Biological Chemistry*, Vol. 279, No. 14, pp. 13817-13824.

Vaccari, I., G. Dina, H. Tronchère, E. Kaufman, G. Chicanne, F. Cerri, L. Wrabetz, B. Payrastre, A. Quattrini, L.S. Weisman *et al.*, 2011, "Genetic Interaction Between MTMR2 and FIG4 Phospholipid Phosphatases Involved in Charcot-Marie-Tooth Neuropathies", *PLoS Genetics*, Vol. 7, No. 10, e1002319.

Velichkova, M., J. Juan, P. Kadandale, S. Jean, I. Riberio, V. Raman, C. Stefan, and A.A. Kiger, 2010, "*Drosophila* Mtm and Class II PI3K Coregulate a PI(3)P Pool with Cortical and Endolysosomal Functions", *The Journal of Cell Biology*, Vol. 190, No. 3, pp. 407-425.

Venken, K.J. and H.J. Bellen, 2005, "Emerging Technologies for Gene Manipulation in *Drosophila melanogaster*", *Nature Reviews Genetics*, Vol. 6, No.3, pp. 167-178.

Venken, K.J., J.H. Simpsons, and H.J. Bellen, 2011, "Genetic Manipulation of Genes and Cells in the Nervous System of the Fruit Fly", *Neuron*, Vol. 72, No. 2, pp. 202-230.

Vermeulen, A., L. Behlen, A. Reynolds, A. Wolfson, W.S. Marshall, J. Karpilow, and A. Khvorova, 2005, "The Contributions of dsRNA Structure to Dicer Specificity and Efficiency", *RNA*, Vol. 11, No. 5, pp. 674-682.

Verny, C., N. Ravise, A.L. Leutenegger, F. Pouplard, O. Dubourg, S. Tardieu, F. Dubas, A. Brice, E. Genin, and E. LeGuern, 2004, "Coincidence of Two Genetic Forms of Charcot-Marie-Tooth Disease in a Single Family", *Neurology*, Vol. 63, No. 8, pp. 1527-1529.

Verstreken, P., T. Ohyama, and H.J. Bellen, 2008, "FM 1–43 Labeling of Synaptic Vesicle Pools at the *Drosophila* Neuromuscular Junction", *Methods in Molecular Biology*, Vol. 440, No. 1, pp. 349-369.

Whitworth, A.J., 2011, "*Drosophila* Models of Parkinson's Disease", *Advances in Genetics*, Vol. 73, No. 1, pp 1-50.

Wishart, M.J. and J.E. Dixon, 2002, “PTEN and Myotubularin Phosphatases: from 3-Phosphoinositide Dephosphorylation to Disease”, *Trends in Cell Biology*, Vol. 12, No. 12, pp. 579-585.

Zala, D., M.V. Hinckelmann, and F. Saudou, 2013, “Huntingtin's Function in Axonal Transport is Conserved in *Drosophila melanogaster*”, *Plos One*, Vol. 8, No. 3, p. e60162.